

Mean-field theory of interacting triplons in a two-dimensional valence-bond solid

R. L. Doretto

Instituto de Física Gleb Wataghin, Universidade Estadual de Campinas, 13083-859 Campinas, SP, Brazil

(Dated: July 14, 2022)

We study a system of interacting triplons (the elementary excitations of a valence-bond solid) described by an effective interacting boson model derived within the bond-operator formalism. In particular, we consider the square lattice spin-1/2 J_1 - J_2 antiferromagnetic Heisenberg model, focus on the intermediate parameter region, where a quantum paramagnetic phase sets in, and consider the columnar valence-bond solid phase. Within the bond-operator theory, the Heisenberg model is mapped into an effective boson model in terms of triplet operators t . The effective boson model is studied at the harmonic approximation and the energy of the triplons and the expansion of the triplon operators b in terms of the triplet operators t are determined. Such an expansion allows us to perform a second mapping, and therefore, determine an effective interacting boson model in terms of the triplon operators b . We then consider systems with a fixed number \bar{N} of triplons and determined the ground-state energy and the spectrum of elementary excitations within a mean-field approximation. We show that many-triplon states are stable, the lowest-energy ones are constituted by a small number of triplons, and the excitation gaps are finite. For $J_2 = 0.48J_1$ and $J_2 = 0.52J_1$, we also calculate spin-spin and dimer-dimer correlation functions, dimer order parameters, and the bipartite von Neumann entanglement entropy within our mean-field formalism in order to determine the properties of the many-triplon state as a function of the triplon number \bar{N} . We find that the spin and the dimer correlations decay exponentially and that the entanglement entropy obeys an area law, regardless the triplon number \bar{N} . Moreover, only for $J_2 = 0.48J_1$, the spin correlations indicate that the many-triplon states with large triplon number \bar{N} might display a more homogeneous singlet pattern than the columnar valence-bond solid. We comment on possible relations between the many-triplon states with large triplon number \bar{N} and gapped spin-liquid states.

I. INTRODUCTION

A valence-bond solid (VBS) is a quantum paramagnetic (disordered) phase that can be realized in a quantum spin system, characterized by the absence of magnetic long-range order, but broken lattice symmetries [1]. Such a state can be viewed as a regular arrangement of singlets that are formed by a set of neighbor spins in a given lattice. An interesting example is the columnar VBS state on a square lattice illustrated in Fig. 1(a): here, nearest-neighbor $S = 1/2$ spins are combined into a singlet (dimer) state, the unit cell has two sites, and both translational and rotational lattice symmetries are broken.

In two-dimensional quantum spin systems, VBS phases have been studied since the seminal work of Read and Sachdev [2]. In particular, two-dimensional frustrated quantum antiferromagnets (AFMs) [3] can, in principle, host VBS phases, since here the interplay between frustration and quantum fluctuations could destroy magnetic long-range order. For instance, for the square lattice spin-1/2 J_1 - J_2 AFM Heisenberg model, it was proposed that the ground state within the intermediate parameter region $0.4J_1 \lesssim J_2 \lesssim 0.6J_1$ could be either a (dimerized) columnar VBS or a (tetramerized) plaquette VBS (see Sec. III below for more details). Interesting, for the same model but on the *honeycomb* lattice, density matrix renormalization group (DMRG) calculations [4, 5] indicate that the ground state of the model is a dimerized VBS for $J_2 \gtrsim 0.36J_1$ [6]. A third example of a frustrated two-dimensional quantum magnet is the spin-1/2 nearest-neighbor AFM Heisenberg model on the kagome

lattice. Here, a dimerized VBS with a 36-site unit cell has been proposed as the ground state [7–9]. Although it has been receiving a lot of attention in recent years (see, e.g., Ref. [10] and the references therein), the ground state of the AFM Heisenberg model on the kagome lattice is still under debate: in addition to the dimerized VBS with a 36-site unit cell, gapped and gapless spin-liquid states [11, 12] have also been proposed.

In addition to the above frustrated two-dimensional AFMs, the nonfrustrated J - Q model also hosts a dimerized VBS phase [13–16]. The J - Q model describes $S = 1/2$ spins on a square lattice interacting via a nearest-neighbor AFM Heisenberg (J) term and an additional four-spin (Q) term within each plaquette. Since it is a nonfrustrated quantum spin system, such a model is free from the so-called sign-problem [17], and therefore, it can be studied within quantum Monte Carlo (QMC) simulations. It was found that a columnar VBS phase sets in for small exchange coupling J , while a Néel magnetic long-range order phase is stable for large J , with the Néel-VBS quantum phase transition (QPT) taking place at $J_c = 0.0447Q$ [14]. Indeed, QMC simulations for the J - Q model [13, 14, 16] indicate that the Néel-VBS is a continuous QPT, in agreement with the deconfined quantum criticality scenario [18]: recall that, within the Landau-Ginzburg framework, the Néel-VBS should be a first-order QPT, since the Néel and the VBS phases are described by two distinct order parameters.

The elementary excitations of a dimerized VBS phase correspond to singlets turned into triplets, the so-called *triplons*. Such excitations can be analytically described, for instance, within the bond-operator representation

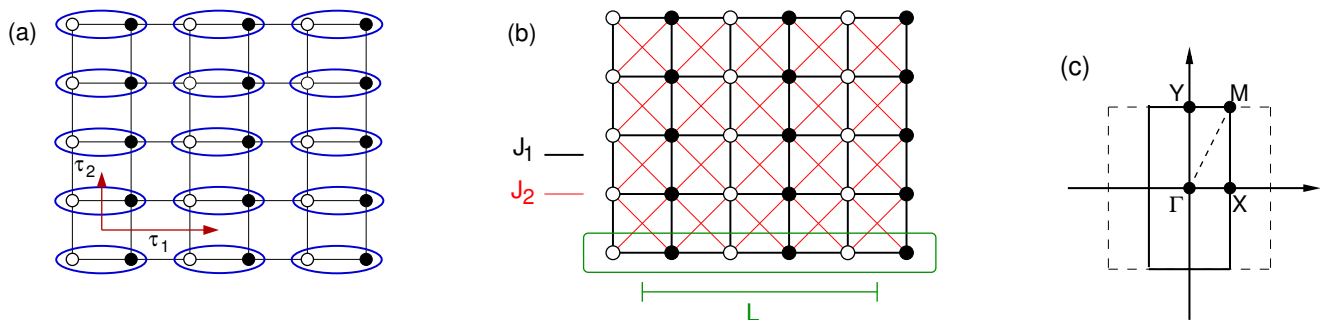


FIG. 1. Schematic representations of (a) the columnar VBS ground state and (b) the square lattice spin-1/2 J_1 - J_2 AFM Heisenberg model (5). The blue ellipses indicate that the spins S^1 (open circle) and S^2 (filled circle) form a singlet state and τ_1 and τ_2 are the primitive vectors of the dimerized lattice \mathcal{D} defined by the (blue) singlets. The green rectangle indicates the one-dimensional subsystem A (dimer chain of size L) considered in the calculations of the entanglement entropy. (c) Brillouin zones of the dimerized (solid line) and the original square (dashed line) lattices. Here $\mathbf{X} = (\pi/2, 0)$, $\mathbf{M} = (\pi/2, \pi)$, and $\mathbf{Y} = (0, \pi)$. The lattice spacing a of the original square lattice is set to 1.

[19], where spin operators are expanded in terms of singlet (s) and triplet (t) boson operators. This formalism follows the ideas of the Holstein-Primakoff representation for spins [20], which describes fluctuations (spin-waves) above a (semiclassical) ground state with magnetic long-range order. The bond-operator representation, however, describes fluctuations above a quantum paramagnetic ground state. For a VBS phase, the bond-operator formalism allows us to map a spin Hamiltonian into an interacting Hamiltonian in terms of triplet operators t , as exemplified below. From the lowest-order (quadratic) terms of the interacting triplet Hamiltonian, we determine the *triplon* (boson) operators b in terms of the triplet operators t and find the triplon spectrum. The effects of the cubic and quartic triplet-triplet interactions can be perturbatively taken into account (as done, e.g., in Refs. [21] and [22] respectively for a dimerized and a tetramerized VBS phases), and therefore, corrections to the (harmonic) energy of the triplons can be determined. In particular, the procedure employed in Ref. [21] allows us to systematically determine an interacting boson model for the triplons.

In this paper, we study the effective interacting boson model for the triplons b derived within the bond-operator formalism for a given VBS (reference) state. We follow a procedure different from the ones employed in Refs. [21, 22], i.e., we consider systems with a fixed number \bar{N} of *triplons* b and determine its ground-state energy and the spectrum of elementary excitations within a mean-field approximation. One of the motivations for our study is to check whether a state with a large number \bar{N} of triplons b could restore some of the lattice symmetries broken when the VBS state sets in: Once a given number of triplons are excited above the VBS ground state, the triplon-triplon interaction could yield two-triplon bound states with total spin zero; the new ground state should also be formed by a set of singlets, similar to the VBS state, but it should no longer display the original VBS pattern; indeed, short (nearest-neighbor) and long sin-

glets might be present, and therefore, some of the lattice symmetries might be restored; in principle, this new ground state (*many-triplon state*) could be a spin-liquid state. In order to discuss such a scenario, we consider, in particular, the spin-1/2 J_1 - J_2 AFM Heisenberg model on the square lattice, since, in principle, it can host a VBS phase. Moreover, we concentrate on a columnar VBS phase, which is considered as the reference state. In addition to discuss the stability of a possible many-triplon state, we also determine its features in terms of the triplon number \bar{N} : the corresponding spin-spin and dimer-dimer correlation functions, dimer order parameters, and the bipartite von-Neumann entanglement entropy are determined within our mean-field formalism.

Our paper is organized as follows: In Sec. II, we briefly summarize the bond-operator representation [19] for spin operators. A short review about the square lattice spin-1/2 J_1 - J_2 AFM Heisenberg model is presented in Sec. III. In Sec. IV, an effective boson model in terms of the triplet operators t for the columnar VBS phase is derived and it is studied within the (lowest-order) harmonic approximation. Here, we define the triplon (boson) operators b in terms of the triplet (boson) operators t and determine the energy of the triplons. An effective interacting boson model for the triplon operators b is derived in Sec. V. We then consider systems with a fixed number \bar{N} of triplons, discuss the stability of the many-triplon states, and determine the excitation spectra within a mean-field approximation. In Sec. VI, spin-spin and dimer-dimer correlation functions and dimer order parameters of the columnar VBS ground state and the many-triplon state with different values of the triplon number \bar{N} are determined. Sec. VII is devoted to the calculation of the bipartite von Neumann entanglement entropy of the columnar VBS ground state and the many-triplon states. Here a one-dimensional (line) subsystem is considered, a choice that allows us to analytically determine the entanglement entropies. We comment on possible implications of our results for the J_1 - J_2 model and provide a brief summary

of our main findings in Sec VIII. Some details of the results discussed in the main text are presented in the two Appendices.

II. BOND OPERATOR REPRESENTATION

We start by briefly reviewing the bond-operator representation for spins introduced by Sachdev and Bhatt [19]. Our summary closely follows the lines of Ref. [23].

Let us consider the Hilbert space of two $S = 1/2$ spins, \mathbf{S}^1 and \mathbf{S}^2 , which is made out of a singlet and three triplet states,

$$\begin{aligned} |s\rangle &= \frac{1}{\sqrt{2}} (|\uparrow\downarrow\rangle - |\downarrow\uparrow\rangle), & |t_x\rangle &= \frac{1}{\sqrt{2}} (|\downarrow\downarrow\rangle - |\uparrow\uparrow\rangle), \\ |t_y\rangle &= \frac{i}{\sqrt{2}} (|\uparrow\uparrow\rangle + |\downarrow\downarrow\rangle), & |t_z\rangle &= \frac{1}{\sqrt{2}} (|\uparrow\downarrow\rangle + |\downarrow\uparrow\rangle). \end{aligned} \quad (1)$$

One can define a set of boson operators, s^\dagger and t_α^\dagger , with $\alpha = x, y, z$, which respectively creates singlet and triplet states out of a fictitious vacuum $|0\rangle$, i.e.,

$$|s\rangle = s^\dagger |0\rangle \quad \text{and} \quad |t_\alpha\rangle = t_\alpha^\dagger |0\rangle, \quad (2)$$

with $\alpha = x, y, z$. In order to remove unphysical states from the enlarged Hilbert space, the constraint

$$s^\dagger s + \sum_\alpha t_\alpha^\dagger t_\alpha = 1 \quad (3)$$

should be introduced. Then, one calculates the matrix elements of each component of the two spin operators within the basis $|s\rangle$ and $|t_\alpha\rangle$, i.e., one determines $\langle s|S_\alpha^\mu|s\rangle$, $\langle s|S_\alpha^\mu|t_\beta\rangle$, and $\langle t_\gamma|S_\alpha^\mu|t_\beta\rangle$, with $\mu = 1, 2$ and $\alpha, \beta, \gamma = x, y, z$. The set of results allows us to conclude that the components of the spin operators \mathbf{S}^1 and \mathbf{S}^2 can be expressed in terms of the boson operators s^\dagger and t_α^\dagger as

$$S_\alpha^{1,2} = \pm \frac{1}{2} \left(s^\dagger t_\alpha + t_\alpha^\dagger s \mp i \epsilon_{\alpha\beta\gamma} t_\beta^\dagger t_\gamma \right), \quad (4)$$

where $\epsilon_{\alpha\beta\gamma}$ is the completely antisymmetric tensor with $\epsilon_{xyz} = 1$ and the summation convention over repeated indices is considered. One then generalizes the bond-operator representation (4) for the lattice case, and therefore, a spin Hamiltonian can be easily written in terms of the boson operators s_i^\dagger and $t_{i\alpha}^\dagger$.

III. THE J_1 - J_2 SQUARE LATTICE ANTIFERROMAGNET HEISENBERG MODEL

To study a system of interacting triplons, we consider, in particular, the spin-1/2 J_1 - J_2 AFM Heisenberg model on the square lattice,

$$\mathcal{H} = J_1 \sum_{\langle ij \rangle} \mathbf{S}_i \cdot \mathbf{S}_j + J_2 \sum_{\langle\langle ij \rangle\rangle} \mathbf{S}_i \cdot \mathbf{S}_j, \quad (5)$$

where \mathbf{S}_i is a spin-1/2 operator at site i and $J_1 > 0$ and $J_2 > 0$ are, respectively, the nearest-neighbor and next-nearest-neighbor exchange couplings, see Fig. 1(b).

It is well known that [22, 24–39], at temperature $T = 0$, the model (5) has a semiclassical Néel magnetic long-range ordered (LRO) phase with ordering wave vector $\mathbf{Q} = (\pi, \pi)$ for $J_2 \lesssim 0.4 J_1$, a collinear magnetic LRO phase with $\mathbf{Q} = (\pi, 0)$ or $(0, \pi)$ for $J_2 \gtrsim 0.6 J_1$, and a quantum paramagnetic phase for $0.4 J_1 \lesssim J_2 \lesssim 0.6 J_1$. The nature of the quantum paramagnetic phase is still under debate. Indeed, several proposals have been made for the ground state of the model (5) within this intermediate parameter region: a (dimerized) columnar VBS [Fig. 1(a)], where both translational and rotational lattice symmetries are broken [29, 30], a (dimerized) staggered VBS [31], a (tetramerized) plaquette VBS, where only the translational lattice symmetry is broken [22, 32, 33], a mixed columnar-plaquette VBS [34], and gapless [35–38] and gapped [39] spin-liquid ground states. Moreover, while there are indications that the quantum paramagnetic-collinear is a first-order QPT, it is not clear whether the Néel-quantum paramagnetic QPT is a first-order or a continuous transition [40].

In the following, we concentrate on the intermediate parameter region $0.4 J_1 \lesssim J_2 \lesssim 0.6 J_1$ and, in particular, consider the columnar VBS phase [Fig. 1(a)].

IV. EFFECTIVE BOSON MODEL I

In this section, we consider the bond-operator representation (4) and derive an effective boson Hamiltonian in terms of the triplet operators $t_{i\alpha}$ to describe the columnar VBS phase of the Heisenberg model (5).

We start rewriting the Hamiltonian (5) in terms of the underline dimerized lattice \mathcal{D} defined by the singlets (dimers) as shown in Fig. 1(a),

$$\begin{aligned} \mathcal{H} = \sum_{i \in \mathcal{D}} J_1 (\mathbf{S}_i^1 \cdot \mathbf{S}_i^2 + \mathbf{S}_i^1 \cdot \mathbf{S}_{i+2}^1 + \mathbf{S}_i^2 \cdot \mathbf{S}_{i+2}^2 + \mathbf{S}_i^2 \cdot \mathbf{S}_{i+1}^1) \\ + J_2 (\mathbf{S}_i^1 \cdot \mathbf{S}_{i+2}^2 + \mathbf{S}_i^2 \cdot \mathbf{S}_{i+2}^1) \\ + J_2 (\mathbf{S}_i^2 \cdot \mathbf{S}_{i+1+2}^1 + \mathbf{S}_i^2 \cdot \mathbf{S}_{i+1-2}^1). \end{aligned} \quad (6)$$

Here, i is a site of the dimerized lattice \mathcal{D} , which has two spins per unit cell (\mathbf{S}_i^1 and \mathbf{S}_i^2), and the index $n = 1, 2$ corresponds to the dimer nearest-neighbor vectors $\boldsymbol{\tau}_n$,

$$\boldsymbol{\tau}_1 = 2a\hat{x}, \quad \boldsymbol{\tau}_2 = a\hat{y}, \quad (7)$$

with a being the lattice spacing of the *original* square lattice. Hereafter, we set $a = 1$.

An effective model in terms of the singlet s_i and triplet $t_{i\alpha}$ boson operators can be obtained by substituting the bond-operator representation (4) generalized to the lattice case into the Hamiltonian (6). It is easy to show that the Hamiltonian (6) assumes the form

$$\mathcal{H} = \mathcal{H}_0 + \mathcal{H}_2 + \mathcal{H}_3 + \mathcal{H}_4, \quad (8)$$

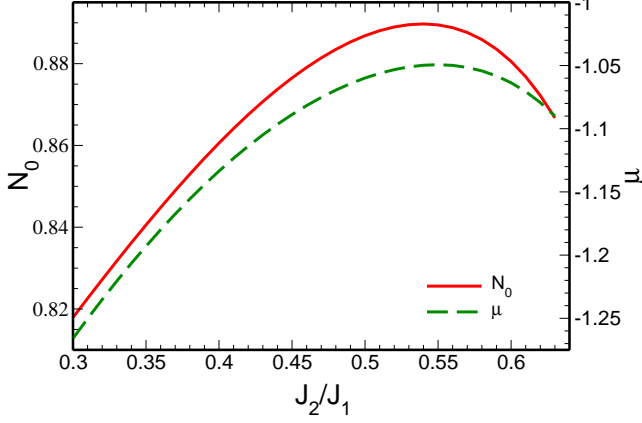


FIG. 2. Parameters N_0 and μ as a functions of J_2/J_1 for the columnar VBS ground state (harmonic approximation) determined from the numerical solutions of the self-consistent equations (25).

where the \mathcal{H}_n terms contain n triplet operators [for details, see Eq. (A1)]. Moreover, we consider the constraint (3) on average via a Lagrange multiplier μ , i.e., we add the following term to the Hamiltonian (8)

$$-\mu \sum_i \left(s_i^\dagger s_i + t_{i\alpha}^\dagger t_{i\alpha} - 1 \right).$$

Within the bond-operator formalism, the columnar VBS ground state [Fig. 1(a)] can be viewed as a condensate of the singlets s_i . Therefore, one sets

$$s_i^\dagger = s_i = \langle s_i^\dagger \rangle = \langle s_i \rangle \rightarrow \sqrt{N_0} \quad (9)$$

in the Hamiltonian (8) and ends up with an effective boson Hamiltonian only in terms of the triplet boson operators $t_{i\alpha}$. As discussed below, the constants N_0 and μ are self-consistently determined for a fixed value of the ratio J_2/J_1 of the exchange couplings.

Finally, considering the Fourier transform,

$$t_{i\alpha}^\dagger = \frac{1}{\sqrt{N'}} \sum_{\mathbf{k} \in \text{BZ}} e^{-i\mathbf{k} \cdot \mathbf{R}_i} t_{\mathbf{k}\alpha}^\dagger, \quad (10)$$

where \mathbf{R}_i is a vector of the dimerized lattice \mathcal{D} , $N' = N/2$ is the number of dimers (N is the number of sites of the original square lattice), and the momentum sum runs over the dimerized first Brillouin zone [Fig. 1(c)], we find that, in momentum space, the four terms \mathcal{H}_n of the

Hamiltonian (8) read

$$\mathcal{H}_0 = -\frac{3}{8} J_1 N N_0 - \frac{1}{2} \mu N (N_0 - 1), \quad (11)$$

$$\mathcal{H}_2 = \sum_{\mathbf{k}} \left[A_{\mathbf{k}} t_{\mathbf{k}\alpha}^\dagger t_{\mathbf{k}\alpha} + \frac{1}{2} B_{\mathbf{k}} \left(t_{\mathbf{k}\alpha}^\dagger t_{-\mathbf{k}\alpha}^\dagger + \text{H.c.} \right) \right], \quad (12)$$

$$\mathcal{H}_3 = \frac{1}{2\sqrt{N'}} \epsilon_{\alpha\beta\lambda} \sum_{\mathbf{p}, \mathbf{k}} \xi_{\mathbf{k}-\mathbf{p}} t_{\mathbf{k}-\mathbf{p}\alpha}^\dagger t_{\mathbf{p}\beta}^\dagger t_{\mathbf{k}\lambda} + \text{H.c.}, \quad (13)$$

$$\mathcal{H}_4 = \frac{1}{2N'} \epsilon_{\alpha\beta\lambda} \epsilon_{\alpha\mu\nu} \sum_{\mathbf{q}, \mathbf{p}, \mathbf{k}} \gamma_{\mathbf{k}} t_{\mathbf{p}+\mathbf{k}\beta}^\dagger t_{\mathbf{q}-\mathbf{k}\mu}^\dagger t_{\mathbf{q}\nu} t_{\mathbf{p}\lambda}, \quad (14)$$

with the coefficients $A_{\mathbf{k}}$, $B_{\mathbf{k}}$, $\xi_{\mathbf{k}}$, and $\gamma_{\mathbf{k}}$ given by

$$A_{\mathbf{k}} = \frac{1}{4} J_1 - \mu + B_{\mathbf{k}}, \quad (15)$$

$$B_{\mathbf{k}} = -\frac{1}{2} N_0 [J_1 \cos(2k_x) - 2(J_1 - J_2) \cos(k_y) + J_2 \cos(2k_x + k_y) + J_2 \cos(2k_x - k_y)], \quad (16)$$

$$\xi_{\mathbf{k}} = -\sqrt{N_0} [J_1 \sin(2k_x) + J_2 \sin(2k_x + k_y) + J_2 \sin(2k_x - k_y)], \quad (17)$$

$$\gamma_{\mathbf{k}} = -\frac{1}{2} [J_1 \cos(2k_x) + 2(J_1 + J_2) \cos k_y + J_2 \cos(2k_x + k_y) + J_2 \cos(2k_x - k_y)]. \quad (18)$$

We should mention that the results presented in this section and in Sec. IV A below were previously quoted in Appendix D from Ref. [22]. Here, however, we derive them in details following, e.g., the lines of Ref. [23].

A. Harmonic approximation

Let us consider the effective boson model (8) in the lowest-order (harmonic) approximation. Here, we only keep the terms of the Hamiltonian (8) up to the quadratic order in the boson operators $t_{\mathbf{k}\alpha}$,

$$\mathcal{H}_2^{\text{HM}} \approx \mathcal{H}_0 + \mathcal{H}_2. \quad (19)$$

Since the Hamiltonian $\mathcal{H}_2^{\text{HM}}$ is quadratic in the triplet operators $t_{\mathbf{k}\alpha}$, it can be diagonalized by the Bogoliubov transformation

$$\begin{aligned} t_{\mathbf{k}\alpha} &= u_{\mathbf{k}} b_{\mathbf{k}\alpha} - v_{\mathbf{k}} b_{-\mathbf{k}\alpha}^\dagger, \\ t_{-\mathbf{k}\alpha}^\dagger &= u_{\mathbf{k}} b_{-\mathbf{k}\alpha}^\dagger - v_{\mathbf{k}} b_{\mathbf{k}\alpha}. \end{aligned} \quad (20)$$

We find that

$$\mathcal{H}_2^{\text{HM}} = E_0^{\text{HM}} + \sum_{\mathbf{k}, \alpha} \omega_{\mathbf{k}} b_{\mathbf{k}\alpha}^\dagger b_{\mathbf{k}\alpha}, \quad (21)$$

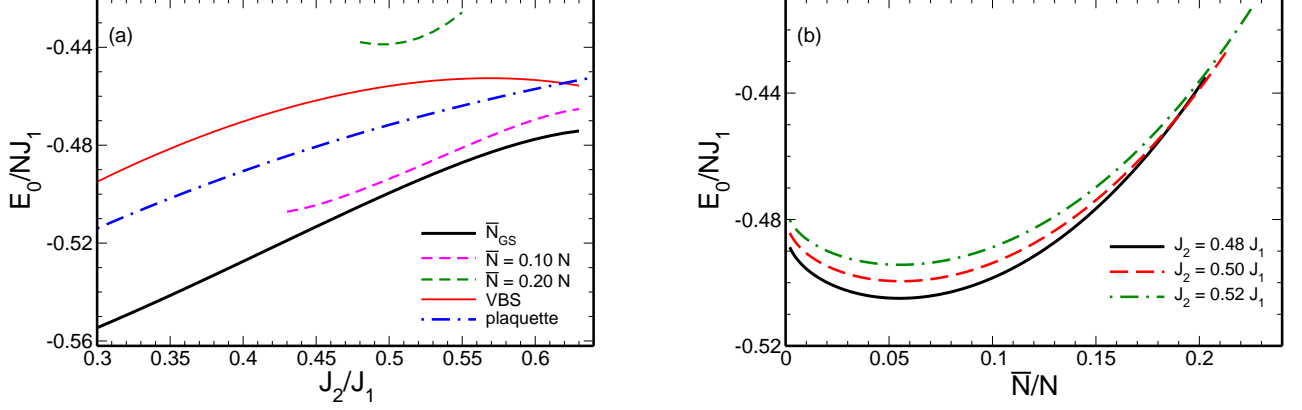


FIG. 3. (a) The energies E_0 [Eq. (42)] per site in terms of J_2/J_1 of the many-triplon state (47) with the triplon number $\bar{N} = \bar{N}_{GS}$ (thick solid black line), $\bar{N} = 0.10 N$ (dashed magenta line), and $\bar{N} = 0.20 N$ (dashed green line). The corresponding harmonic results for the columnar VBS ground state E_0^{HM} [Eq. (22)] (thin solid red line) and for the plaquette VBS ground state (Ref. [22]) (dotted-dashed blue line) are also included. (b) The energies E_0 [Eq. (42)] per site in terms of \bar{N}/N of the many-triplon state (47) for $J_2 = 0.48 J_1$ (solid black line), $J_2 = 0.50 J_1$ (dashed red line), and $J_2 = 0.52 J_1$ (dotted-dashed green line).

where

$$E_0^{HM} = -\frac{3}{8}J_1 N N_0 - \frac{1}{2}\mu N(N_0 - 1) + \frac{3}{2}\sum_{\mathbf{k}}(\omega_{\mathbf{k}} - A_{\mathbf{k}}) \quad (22)$$

is the ground-state energy,

$$\omega_{\mathbf{k}} = \sqrt{A_{\mathbf{k}}^2 - B_{\mathbf{k}}^2} \quad (23)$$

is the energy of the *triplons* (the elementary excitations above the VBS ground state |VBS>), and the coefficients $u_{\mathbf{k}}$ and $v_{\mathbf{k}}$ of the Bogoliubov transformation (20) read

$$u_{\mathbf{k}}^2, v_{\mathbf{k}}^2 = \frac{1}{2} \left(\frac{A_{\mathbf{k}}}{\omega_{\mathbf{k}}} \pm 1 \right), \quad \text{and} \quad u_{\mathbf{k}} v_{\mathbf{k}} = \frac{B_{\mathbf{k}}}{2\omega_{\mathbf{k}}}. \quad (24)$$

The constants μ and N_0 are calculated from the saddle-point conditions $\partial E_0^{HM}/\partial N_0 = 0$ and $\partial E_0^{HM}/\partial \mu = 0$, and therefore, we find a set of self-consistent equations,

$$\mu = -\frac{3J_1}{4} + \frac{3}{2N_0} \frac{1}{N'} \sum_{\mathbf{k}} B_{\mathbf{k}} \left(\frac{A_{\mathbf{k}} - B_{\mathbf{k}}}{\omega_{\mathbf{k}}} - 1 \right), \quad (25)$$

$$N_0 = 1 - \frac{1}{N'} \sum_{\mathbf{k}\alpha} \langle t_{\mathbf{k}\alpha}^\dagger t_{\mathbf{k}\alpha} \rangle = 1 + \frac{3}{2N'} \sum_{\mathbf{k}} \left(1 - \frac{A_{\mathbf{k}}}{\omega_{\mathbf{k}}} \right),$$

that are solved for a fixed value of the ratio J_2/J_1 . Note that, once the constants μ and N_0 are calculated, the ground-state energy (22) and the triplon dispersion relation (23) are completely determined.

The numerical solutions of the set of self-consistent equations (25) are shown in Fig. 2, where the parameters μ and N_0 are plotted as a function of J_2/J_1 . One

sees that N_0 and μ monotonically increases with J_2/J_1 up to $J_2 = 0.55 J_1$. Moreover, one notices that, within the harmonic approximation, the columnar VBS phase is stable for $0.30 J_1 \leq J_2 \leq 0.63 J_1$, i.e., a parameter region larger than the one ($0.4 J_1 \lesssim J_2 \lesssim 0.6 J_1$) expected for the disordered phase of the model (5) (see Sec. III). Such a feature of the harmonic approximation was found in our previous studies [21–23].

Figure 3(a) shows the ground-state energy (22) in terms of the ratio J_2/J_1 . Similar to the parameters μ and N_0 , the ground-state energy E_0^{HM} monotonically increases with J_2/J_1 , but up to $J_2 = 0.57 J_1$. For comparison, the ground-state energy of the plaquette VBS phase determined within an harmonic approximation (Ref. [22]) is also included. One sees that, within the corresponding harmonic approximations, the (tetramerized) plaquette VBS ground state has lower energy than the (dimerized) columnar VBS one. Finally, we should mention that E_0^{HM} of the columnar VBS ground state was also previously reported in Ref. [22]. However, we found a mistake in our previous numerical code, and therefore, the results shown in Fig. 3(a) are indeed the correct ones.

The triplon excitation spectrum $\omega_{\mathbf{k}}$ [Eq. (23)] of the columnar VBS phase for $J_2 = 0.48 J_1$ is shown in Fig. 4(a). As expected for a disordered phase, the triplon excitation spectrum is gapped. Moreover, one notices that the triplon gap (the minimum of the dispersion relation $\omega_{\mathbf{k}}$) is located at the $\mathbf{Y} = (0, \pi)$ point of the first Brillouin zone [Fig. 1(c)]. Indeed, we find that these two features hold for the parameter region $0.30 J_1 \leq J_2 \leq 0.50 J_1$. Similarly, for the parameter region $0.50 J_1 \leq J_2 \leq 0.63 J_1$, we also find a finite triplon excitation gap, but here it is associated with the Γ point

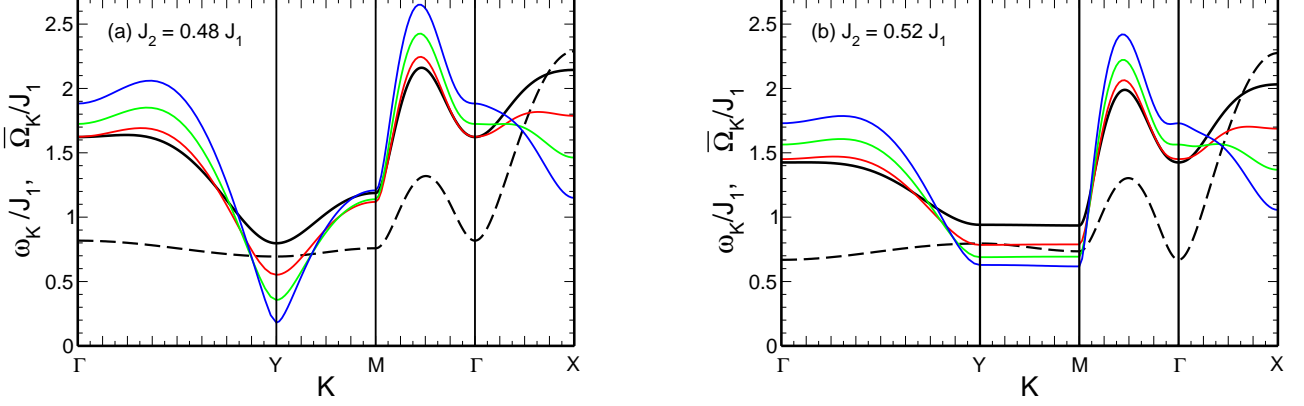


FIG. 4. Triplon dispersion relations $\omega_{\mathbf{k}}$ [Eq. (23)] of the columnar VBS phase at the harmonic approximation (dashed black lines) and the dispersion relations $\bar{\Omega}_{\mathbf{k}}$ [Eq. (43)] of the elementary excitations above the many-triplon state (47) within a mean-field approximation (solid lines) along paths in the dimerized Brillouin zone [Fig. 1(c)] for (a) $J_2 = 0.48 J_1$ and (b) $J_2 = 0.52 J_1$. Results for four different values of \bar{N} are shown: $\bar{N} = \bar{N}_{GS}$ (solid black line), $\bar{N} = 0.10 N$ (solid red line), $\bar{N} = 0.15 N$ (solid green line), and $\bar{N} = 0.20 N$ (solid blue line).

(the centre of the first Brillouin zone), as exemplified in Fig. 4(b) for $J_2 = 0.52 J_1$. The complete behaviour of the triplon gap as a function of J_2/J_1 is shown in Fig. 5. We should note that, for the first and second parameter regions above mentioned, the momenta associated with the triplon gap are respectively equal to the ordering wave vectors \mathbf{Q} of the Néel and collinear magnetic long-range ordered phases that set in for small and large J_2 (see Sec. III). As discussed, e.g., in Refs. [21, 22], the vanishing of the triplon gap defines a quantum phase transition to a magnetic ordered phase. Here, the triplon gap determined within the harmonic approximation decreases as we approach the critical couplings $J_{2c} = 0.30 J_1$ and $J_{2c} = 0.63 J_1$, but it does not vanish.

As mentioned in Sec. I, the effects of the cubic [Eq. (13)] and the quartic [Eq. (14)] triplet-triplet interactions can be perturbatively taken into account and corrections to the harmonic results obtained. In particular, such effects could decrease the triplon excitation gap and, eventually, it could vanish at different critical couplings J_{2c} . In this case, the closing of the triplon gap determines the region of stability of the VBS phase which, in general, is smaller than the one determined within the harmonic approximation (see, e.g., Fig. 10 of Ref. [21] and Fig. 7 of Ref. [22]). Here, instead of determining corrections to the harmonic results, we follow a different route, consider the triplons b as defined by the harmonic approximation [Eqs. (20) and (24)], and study a system with a fixed number \bar{N} of triplons.

V. EFFECTIVE BOSON MODEL II

Once the triplon operators $b_{\mathbf{k}\alpha}$ are defined in terms of the triplet operators $t_{\mathbf{k}\alpha}$ [Eq. (20)] and the triplon spectrum (23) and the triplon vacuum |VBS> are determined within the harmonic approximation, we now consider a system with a fixed number \bar{N} of triplons.

We start expressing the effective boson model (8) in terms of the boson operators $b_{\mathbf{k}\alpha}$, i.e., we derive an effective boson model for the triplons b . With the aid of the Bogoliubov transformation (20), one shows that the cubic term (13) can be written in terms of the b operators as [21]

$$\begin{aligned} \mathcal{H}_3 = & \frac{1}{2\sqrt{\bar{N}'}} \sum_{\mathbf{k}, \mathbf{p}} \sum_{\alpha, \beta, \gamma}' \Xi_1(\mathbf{k}, \mathbf{p}) (b_{\mathbf{k}-\mathbf{p}\alpha}^\dagger b_{\mathbf{p}\beta}^\dagger b_{\mathbf{k}\gamma} + \text{H.c.}) \\ & + \frac{1}{2\sqrt{\bar{N}'}} \sum_{\mathbf{k}, \mathbf{p}} \Xi_2(\mathbf{k}, \mathbf{p}) (b_{\mathbf{k}-\mathbf{p}x}^\dagger b_{\mathbf{p}y}^\dagger b_{-\mathbf{k}z}^\dagger + \text{H.c.}). \end{aligned} \quad (26)$$

Here, the sum over α, β, γ has only three components, $(\alpha, \beta, \gamma) = (x, y, z)$, (z, x, y) , and (y, z, x) , the renormalized vertex $\Xi_1(\mathbf{k}, \mathbf{p})$ reads

$$\begin{aligned} \Xi_1(\mathbf{k}, \mathbf{p}) = & (\xi_{\mathbf{k}-\mathbf{p}} - \xi_{\mathbf{p}}) (u_{\mathbf{k}-\mathbf{p}} u_{\mathbf{p}} u_{\mathbf{k}} + v_{\mathbf{k}-\mathbf{p}} v_{\mathbf{p}} v_{\mathbf{k}}) \\ & + (\xi_{\mathbf{k}} + \xi_{\mathbf{p}}) (v_{\mathbf{k}-\mathbf{p}} u_{\mathbf{p}} v_{\mathbf{k}} + u_{\mathbf{k}-\mathbf{p}} v_{\mathbf{p}} u_{\mathbf{k}}) \\ & - (\xi_{\mathbf{k}-\mathbf{p}} + \xi_{\mathbf{k}}) (v_{\mathbf{k}-\mathbf{p}} u_{\mathbf{p}} u_{\mathbf{k}} + u_{\mathbf{k}-\mathbf{p}} v_{\mathbf{p}} v_{\mathbf{k}}), \end{aligned} \quad (27)$$

with $\xi_{\mathbf{k}}$ being the bare cubic vertex (17) and $u_{\mathbf{k}}$ and $v_{\mathbf{k}}$ being the Bogoliubov coefficients (24). The vertex $\Xi_2(\mathbf{k}, \mathbf{p}) = -\Xi_1(\mathbf{k}, \mathbf{p})$ with the replacements $u_{\mathbf{k}} \leftrightarrow v_{\mathbf{k}}$.

Following the same procedure for the quartic term (14), one shows, after normal-ordering, that

$$\mathcal{H}_4 = E_{40} + \mathcal{H}_{24} + \mathcal{H}_{44}, \quad (28)$$

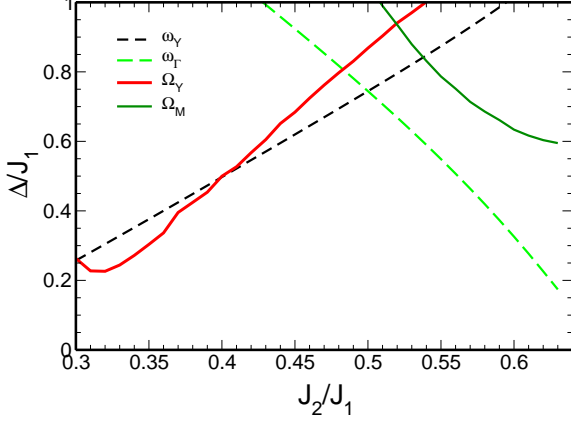


FIG. 5. Harmonic excitation gap (dashed lines) of the columnar VBS phase and the excitation gap (solid lines) above the many-triplon state (47) with $\bar{N} = \bar{N}_{GS}$ as a function of J_2/J_1 . ω_Y (black dashed line) and ω_Γ (green dashed line) are respectively the energies $\omega_{\mathbf{k}}$ [Eq. (23)] of the triplon at the $\mathbf{Y} = (0, \pi)$ and the Γ points of the dimerized Brillouin zone; $\bar{\Omega}_Y$ (solid red line) and $\bar{\Omega}_M$ (solid dark green line) are respectively the energies $\bar{\Omega}_{\mathbf{k}}$ [Eq. (43)] of the elementary excitations above the many-triplon state (47) with $\bar{N} = \bar{N}_{GS}$ at the $\mathbf{Y} = (0, \pi)$ and the $\mathbf{M} = (\pi/2, \pi)$ points of the dimerized Brillouin zone.

where

$$E_{40} = \frac{3}{N'} \sum_{\mathbf{k}, \mathbf{p}} \gamma_{\mathbf{k}-\mathbf{p}} (u_{\mathbf{k}} v_{\mathbf{k}} u_{\mathbf{p}} v_{\mathbf{p}} - v_{\mathbf{k}}^2 v_{\mathbf{p}}^2), \quad (29)$$

$$\mathcal{H}_{24} = \sum_{\mathbf{k}} \left[A_{\mathbf{k}}^{(4)} b_{\mathbf{k}\alpha}^\dagger b_{\mathbf{k}\alpha} + \frac{1}{2} B_{\mathbf{k}}^{(4)} (b_{\mathbf{k}\alpha}^\dagger b_{-\mathbf{k}\alpha}^\dagger + \text{H.c.}) \right], \quad (30)$$

and

$$\begin{aligned} \mathcal{H}_{44} = \frac{1}{2N'} \epsilon_{\alpha\beta\lambda} \epsilon_{\alpha\mu\nu} \sum_{\mathbf{q}, \mathbf{p}, \mathbf{k}} [& \\ & \Gamma_1(\mathbf{p}, \mathbf{q}, \mathbf{k}) b_{\mathbf{p}+\mathbf{k}\beta}^\dagger b_{\mathbf{q}-\mathbf{k}\mu}^\dagger b_{-\mathbf{q}\nu}^\dagger b_{-\mathbf{p}\lambda}^\dagger + \text{H.c.} \\ & + \Gamma_2(\mathbf{p}, \mathbf{q}, \mathbf{k}) b_{\mathbf{p}+\mathbf{k}\beta}^\dagger b_{\mathbf{q}-\mathbf{k}\mu}^\dagger b_{-\mathbf{q}\nu}^\dagger b_{\mathbf{p}\lambda} + \text{H.c.} \\ & + \Gamma_3(\mathbf{p}, \mathbf{q}, \mathbf{k}) b_{\mathbf{p}+\mathbf{k}\beta}^\dagger b_{\mathbf{q}-\mathbf{k}\mu}^\dagger b_{\mathbf{q}\nu} b_{\mathbf{p}\lambda} \\ & + \Gamma_4(\mathbf{p}, \mathbf{q}, \mathbf{k}) b_{\mathbf{p}+\mathbf{k}\beta}^\dagger b_{-\mathbf{p}\lambda}^\dagger b_{-\mathbf{q}+\mathbf{k}\mu} b_{\mathbf{q}\nu}]. \quad (31) \end{aligned}$$

Here, the coefficients $A_{\mathbf{k}}^{(4)}$ and $B_{\mathbf{k}}^{(4)}$ are given by

$$A_{\mathbf{k}}^{(4)} = \frac{2}{N'} \sum_{\mathbf{p}} \gamma_{\mathbf{k}-\mathbf{p}} [2u_{\mathbf{k}} v_{\mathbf{k}} u_{\mathbf{p}} v_{\mathbf{p}} - (u_{\mathbf{k}}^2 + v_{\mathbf{k}}^2) v_{\mathbf{p}}^2], \quad (32)$$

$$B_{\mathbf{k}}^{(4)} = \frac{2}{N'} \sum_{\mathbf{p}} \gamma_{\mathbf{k}-\mathbf{p}} [2u_{\mathbf{k}} v_{\mathbf{k}} v_{\mathbf{p}}^2 - (u_{\mathbf{k}}^2 + v_{\mathbf{k}}^2) u_{\mathbf{p}} v_{\mathbf{p}}],$$

and the functions $\Gamma_i(\mathbf{p}, \mathbf{q}, \mathbf{k})$ read

$$\Gamma_1(\mathbf{p}, \mathbf{q}, \mathbf{k}) = \gamma_{\mathbf{k}} u_{\mathbf{p}+\mathbf{k}} u_{\mathbf{q}-\mathbf{k}} v_{\mathbf{q}} v_{\mathbf{p}},$$

$$\Gamma_2(\mathbf{p}, \mathbf{q}, \mathbf{k}) = 2\gamma_{\mathbf{k}} (v_{\mathbf{p}+\mathbf{k}} u_{\mathbf{q}-\mathbf{k}} v_{\mathbf{q}} v_{\mathbf{p}} - u_{\mathbf{p}+\mathbf{k}} u_{\mathbf{q}-\mathbf{k}} v_{\mathbf{q}} u_{\mathbf{p}}),$$

$$\Gamma_3(\mathbf{p}, \mathbf{q}, \mathbf{k}) = \gamma_{\mathbf{k}} (u_{\mathbf{p}+\mathbf{k}} u_{\mathbf{q}-\mathbf{k}} u_{\mathbf{q}} u_{\mathbf{p}} + v_{\mathbf{p}+\mathbf{k}} v_{\mathbf{q}-\mathbf{k}} v_{\mathbf{q}} v_{\mathbf{p}}$$

$$- u_{\mathbf{p}+\mathbf{k}} v_{\mathbf{q}-\mathbf{k}} v_{\mathbf{q}} u_{\mathbf{p}} - v_{\mathbf{p}+\mathbf{k}} u_{\mathbf{q}-\mathbf{k}} u_{\mathbf{q}} v_{\mathbf{p}}),$$

$$\Gamma_4(\mathbf{p}, \mathbf{q}, \mathbf{k}) = 2\gamma_{\mathbf{k}} u_{\mathbf{p}+\mathbf{k}} v_{\mathbf{q}-\mathbf{k}} u_{\mathbf{q}} v_{\mathbf{p}}, \quad (33)$$

with $\gamma_{\mathbf{k}}$ being the bare quartic vertex (18) and $u_{\mathbf{k}}$ and $v_{\mathbf{k}}$, the Bogoliubov coefficients (24). We refer the reader to Eq. (B6) for alternative expressions for the constant E_{40} and the coefficients $A_{\mathbf{k}}^{(4)}$ and $B_{\mathbf{k}}^{(4)}$ that are useful in the self-consistent problem discussed in the next section.

Therefore, the effective (interacting) boson model for the triplons b (considering the columnar VBS as a reference state) assumes the form

$$\mathcal{H} = \mathcal{H}_2^{\text{HM}} + \mathcal{H}_3 + \mathcal{H}_4, \quad (34)$$

where $\mathcal{H}_2^{\text{HM}}$ is the (quadratic) harmonic Hamiltonian (21), and the cubic \mathcal{H}_3 and the quartic \mathcal{H}_4 terms are respectively given by Eqs. (26) and (28).

A. Mean-field approximation

In this section, we study systems with a fixed number \bar{N} of triplons described by the Hamiltonian (34). In particular, we neglected the cubic term \mathcal{H}_3 and consider the quartic term \mathcal{H}_4 within a mean-field approximation. The idea is to verify whether a ground state formed by a certain number of triplons (the *many-triplon state*) is stable, in addition to determine the corresponding excitation spectrum.

It is easy to show that, within a mean-field approximation, the quartic term \mathcal{H}_{44} [Eq. (31)] assumes the form

$$\begin{aligned} \mathcal{H}_{44}^{MF} = E_{44} + \sum_{\mathbf{k}\alpha} [& \\ & \Delta_{1,\mathbf{k}} b_{\mathbf{k}\alpha}^\dagger b_{\mathbf{k}\alpha} \\ & + \frac{1}{2} \Delta_{2,\mathbf{k}} (b_{\mathbf{k}\alpha}^\dagger b_{-\mathbf{k}\alpha}^\dagger + \text{H.c.})], \quad (35) \end{aligned}$$

where the constant E_{44} [Eq. (B7)] and the coefficients $\Delta_{1,\mathbf{k}}$ [Eq. (B8)] and $\Delta_{2,\mathbf{k}}$ [Eq. (B9)] are defined in terms

of the bare quartic vertex $\gamma_{\mathbf{k}}$ [Eq. (18)], the Bogoliubov coefficients $u_{\mathbf{k}}$ and $v_{\mathbf{k}}$ [Eq. (24)], and the normal ($h_{\mathbf{k}}$) and anomalous ($\bar{h}_{\mathbf{k}}$) expectation values:

$$h_{\mathbf{k}} \equiv \langle b_{\mathbf{k}\alpha}^\dagger b_{\mathbf{k}\alpha} \rangle, \quad \bar{h}_{\mathbf{k}} \equiv \langle b_{\mathbf{k}\alpha} b_{-\mathbf{k}\alpha} \rangle. \quad (36)$$

Due to the fact that the quartic term \mathcal{H}_{44} does not conserve the number of particles, one should include not only $h_{\mathbf{k}}$ but also $\bar{h}_{\mathbf{k}}$. Moreover, we consider both normal and anomalous expectation values α independent, since the triplon energy (23) and the quartic vertices $\Gamma_i(\mathbf{p}, \mathbf{q}, \mathbf{k})$ [Eq. (33)] do not depend on the index α .

From Eqs. (21), (29), (30), and (35), we then find that the mean field Hamiltonian for a system of \bar{N} triplons is given by

$$\mathcal{H} = \mathcal{H}^{MF} - \bar{\mu} \bar{N}$$

$$\mathcal{H} = \mathcal{H}_2^{HM} + E_{40} + \mathcal{H}_{24} + \mathcal{H}_{44}^{MF} - \bar{\mu} \bar{N}$$

$$\mathcal{H} = E_0^{HM} + E_{40} + E_{44}$$

$$+ \sum_{\mathbf{k}\alpha} \left[\bar{A}_{\mathbf{k}} b_{\mathbf{k}\alpha}^\dagger b_{\mathbf{k}\alpha} + \frac{1}{2} \bar{B}_{\mathbf{k}} \left(b_{\mathbf{k}\alpha}^\dagger b_{-\mathbf{k}\alpha}^\dagger + \text{H.c.} \right) \right]. \quad (37)$$

Here, the coefficients $\bar{A}_{\mathbf{k}}$ and $\bar{B}_{\mathbf{k}}$ read

$$\begin{aligned} \bar{A}_{\mathbf{k}} &= \omega_{\mathbf{k}} + A_{\mathbf{k}}^{(4)} + \Delta_{1,\mathbf{k}} - \bar{\mu}, \\ \bar{B}_{\mathbf{k}} &= B_{\mathbf{k}}^{(4)} + \Delta_{2,\mathbf{k}}, \end{aligned} \quad (38)$$

with $\omega_{\mathbf{k}}$ being the harmonic triplon energy (23), the coefficients $A_{\mathbf{k}}^{(4)}$ and $B_{\mathbf{k}}^{(4)}$ given by Eq. (32), and the coefficients $\Delta_{1,\mathbf{k}}$ and $\Delta_{2,\mathbf{k}}$ respectively given by Eqs. (B8) and (B9). Moreover, $\bar{\mu}$ is the chemical potential related to the total number of triplons b , i.e.,

$$\bar{N} = \sum_{\mathbf{k}\alpha} b_{\mathbf{k}\alpha}^\dagger b_{\mathbf{k}\alpha}. \quad (39)$$

The Hamiltonian (37) can be diagonalized by a Bogoliubov transformation similar to the transformation (20):

$$\begin{aligned} b_{\mathbf{k}\alpha} &= \bar{u}_{\mathbf{k}} a_{\mathbf{k}\alpha} - \bar{v}_{\mathbf{k}} a_{-\mathbf{k}\alpha}^\dagger, \\ b_{-\mathbf{k}\alpha}^\dagger &= \bar{u}_{\mathbf{k}} a_{-\mathbf{k}\alpha}^\dagger - \bar{v}_{\mathbf{k}} a_{\mathbf{k}\alpha}. \end{aligned} \quad (40)$$

We then arrive at

$$\mathcal{H} = E_0 + \sum_{\mathbf{k}\alpha} \bar{\Omega}_{\mathbf{k}} a_{\mathbf{k}\alpha}^\dagger a_{\mathbf{k}\alpha}, \quad (41)$$

where

$$E_0 = E_0^{HM} + E_{40} + E_{44} + \frac{3}{2} \sum_{\mathbf{k}} (\bar{\Omega}_{\mathbf{k}} - \bar{A}_{\mathbf{k}}) \quad (42)$$

is the energy of the many-triplon state $|\Psi_0\rangle$ [see Eq. (47) below],

$$\bar{\Omega}_{\mathbf{k}} = \sqrt{\bar{A}_{\mathbf{k}}^2 - \bar{B}_{\mathbf{k}}^2} \quad (43)$$

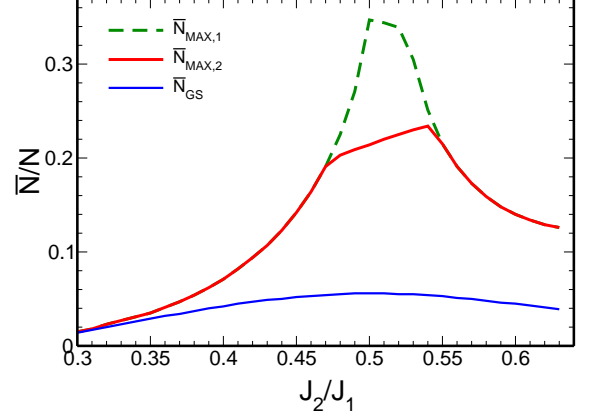


FIG. 6. The parameters $\bar{N}_{MAX,1}$ (dashed green line), $\bar{N}_{MAX,2}$ (thick solid red line), and \bar{N}_{GS} (thin solid blue line) as a function of J_2/J_1 determined from the numerical solutions of the self-consistent problem (B13)-(B15).

is the energy of the elementary excitations above the many-triplon state $|\Psi_0\rangle$, and the coefficients $\bar{u}_{\mathbf{k}}$ and $\bar{v}_{\mathbf{k}}$ of the Bogoliubov transformation (40) are given by

$$\bar{u}_{\mathbf{k}}^2, \bar{v}_{\mathbf{k}}^2 = \frac{1}{2} \left(\frac{\bar{A}_{\mathbf{k}}}{\bar{\Omega}_{\mathbf{k}}} \pm 1 \right) \quad \text{and} \quad \bar{u}_{\mathbf{k}} \bar{v}_{\mathbf{k}} = \frac{\bar{B}_{\mathbf{k}}}{2\bar{\Omega}_{\mathbf{k}}}. \quad (44)$$

From Eqs. (40) and (44), one shows that the normal $h_{\mathbf{k}}$ and anomalous $\bar{h}_{\mathbf{k}}$ expectation values (36) assume the form

$$\begin{aligned} h_{\mathbf{p}} &= \langle b_{\mathbf{p}\alpha}^\dagger b_{\mathbf{p}\alpha} \rangle = \bar{v}_{\mathbf{p}}^2 = \frac{1}{2} \left(-1 + \frac{\bar{A}_{\mathbf{p}}}{\bar{\Omega}_{\mathbf{p}}} \right), \\ \bar{h}_{\mathbf{p}} &= \langle b_{\mathbf{p}\alpha} b_{-\mathbf{p}\alpha} \rangle = -\bar{v}_{\mathbf{p}} \bar{u}_{\mathbf{p}} = -\frac{\bar{B}_{\mathbf{p}}}{2\bar{\Omega}_{\mathbf{p}}}. \end{aligned} \quad (45)$$

Moreover, considering the condition (39) on average, Eq. (45) yields

$$\frac{\bar{N}}{N} = \frac{3}{4N'} \sum_{\mathbf{k}} \left(-1 + \frac{\bar{A}_{\mathbf{p}}}{\bar{\Omega}_{\mathbf{p}}} \right), \quad (46)$$

where N is the number of sites of the *original* square lattice. Important, only systems with $\bar{N} \leq N/2$ should be considered.

We determine the normal and anomalous expectation values (45) and the chemical potential $\bar{\mu}$ related to the condition (46) for fixed values of the triplon number \bar{N} and the ratio J_2/J_1 of the exchange couplings by numerically solving the self-consistent problem defined by Eqs. (B13)-(B15). We refer the reader to Appendix B for the details of the self-consistent procedure. Important, for a given value of the ratio J_2/J_1 , we consider the values of the parameter N_0 and the Lagrange multiplier μ determined within the harmonic approximation for the columnar VBS state [Fig. 2], since it is the reference state that defines the triplons b .

Before discussing the numerical results, a few remarks here about the nature of the many-triplon state $|\Psi_0\rangle$ are in order: It is possible to show that the expectation values (45) are consistent with the state

$$|\Psi_0\rangle = C \prod_{\mathbf{k}} \exp\left(-\phi_{\mathbf{k}} b_{-\mathbf{k}\alpha}^\dagger b_{\mathbf{k}\alpha}^\dagger\right) |\text{VBS}\rangle, \quad (47)$$

where $\phi_{\mathbf{k}} = \bar{v}_{\mathbf{k}}/\bar{u}_{\mathbf{k}}$, with $\bar{u}_{\mathbf{k}}$ and $\bar{v}_{\mathbf{k}}$ being the Bogoliubov coefficients (44), the normalization constant $C^{-2} = \prod_{\mathbf{k}} \bar{u}_{\mathbf{k}}^2$, and $|\text{VBS}\rangle$ is the vacuum for the triplons b . Therefore, the many-triplon state (within our mean-field approximation) is a BCS-like state that correlates pairs of triplons b with momenta \mathbf{k} and $-\mathbf{k}$ and the same index $\alpha = x, y, z$. Important, $|\Psi_0\rangle$ does not describe a triplon-pair condensate, since here there is no $U(1)$ symmetry to be broken. Indeed, both the Hamiltonian (34) and the ground state (47) only preserve a Z_2 symmetry: $b_{\mathbf{k}} \rightarrow -b_{\mathbf{k}}$.

For a fixed value of the ratio J_2/J_1 , we find numerical solutions for the self-consistent problem (B13)-(B15) only for $\bar{N} \leq \bar{N}_{MAX,1}$, where the values of the parameter $\bar{N}_{MAX,1}$ as a function of J_2/J_1 are shown in Fig. 6. Important, for $0.48J_1 \leq J_2 \leq 0.54J_1$, we find solutions for the self-consistent problem with

$$N_{\text{Triplet}} = \frac{1}{N'} \sum_{\mathbf{k}\alpha} \langle t_{\mathbf{k}\alpha}^\dagger t_{\mathbf{k}\alpha} \rangle > 1.$$

Taking into account the additional condition $N_{\text{Triplet}} < 1$, we define the parameter $\bar{N}_{MAX,2}$ (see Fig 6), and therefore, we only consider solutions of the self-consistent problem with $\bar{N} \leq \bar{N}_{MAX,2}$.

For a given value of the ratio J_2/J_1 of the exchange couplings, the energy E_0 [Eq. (42)] of the many-triplon state (47) has a non-monotonic behaviour as \bar{N} increases [Fig. 3(b)] and, in particular, it reaches a minimum value at $\bar{N} = \bar{N}_{GS}$, where the values of \bar{N}_{GS} as a function of J_2/J_1 are displayed in Fig. 6. One notices that $\bar{N}_{GS} < 0.056N$, where N is the number of sites of the original square lattice, i.e., the lowest-energy many-triplon state (47) has a small number of triplons b . The behaviour of the energy (42) for $\bar{N} = \bar{N}_{GS}$ as a function of J_2/J_1 is shown in Fig. 3(a). Interesting, one sees that, for a given value of J_2/J_1 , the ground-state energy E_0 of the many-triplon state with $\bar{N} = \bar{N}_{GS}$ is smaller than the ones of the columnar [Eq. (22)] and plaquette (Ref. [22]) VBSs both determined at the corresponding harmonic levels.

Figure 4 shows the energy of the elementary excitations $\bar{\Omega}_{\mathbf{k}}$ [Eq. (43)] above the many-triplon state (47) with $\bar{N} = \bar{N}_{GS}$ for $J_2 = 0.48J_1$ [Fig. 4(a)] and $J_2 = 0.52J_1$ [Fig. 4(b)]. Apart from the momenta close to the X point, one sees that, for both values of the model parameter J_2 , $\bar{\Omega}_{\mathbf{k}} > \omega_{\mathbf{k}}$, where $\omega_{\mathbf{k}}$ is the corresponding (harmonic) triplon energy (23). In particular, for $J_2 = 0.48J_1$, the excitation gap is located at the Y point, the same momentum associated with the triplon gap of the corresponding columnar VBS state [dashed black line,

Fig. 4(a)]. On the other hand, for $J_2 = 0.52J_1$, the excitation gap is located at the M point, different from the corresponding columnar VBS state whose triplon gap is associated with the Γ point [dashed black line, Fig. 4(b)]. Indeed, one finds that the features described above for $J_2 = 0.48J_1$ hold for the parameter region $J_2 \leq 0.51J_1$, while the ones found for $J_2 = 0.52J_1$, for the parameter region $J_2 > 0.51J_1$. The complete behaviour of the excitation gap above the many-triplon state with $\bar{N} = \bar{N}_{GS}$ as a function of J_2/J_1 and a comparison with the (harmonic) excitation gap of the columnar VBS ground state are shown in Fig. 5.

In addition to the lowest-energy many-triplon state (47) with $\bar{N} = \bar{N}_{GS}$, we also consider (high-energy) triplon ground states with larger number of triplons, $\bar{N} > \bar{N}_{GS}$. In particular, in Fig. 3(a), we show the energy (42) of the many-triplon state for $\bar{N} = 0.10N$ and $0.20N$ in terms of J_2/J_1 . As already mentioned, for a given value of the ratio J_2/J_1 , the energy (42) increases with the number of triplons \bar{N} when $\bar{N} > \bar{N}_{GS}$. Figure 4 also displays the spectra of the elementary excitations $\bar{\Omega}_{\mathbf{k}}$ [Eq. (43)] above the many-triplon state (47) for $\bar{N} = 0.10N$, $0.15N$, and $0.20N$ and $J_2 = 0.48J_1$ [Fig. 4(a)] and $J_2 = 0.52J_1$ [Fig. 4(b)]. Apart from the region around the X point, the excitation spectra for $\bar{N} > \bar{N}_{GS}$ have the same (qualitatively) features of the corresponding ones for $\bar{N} = \bar{N}_{GS}$. Moreover, we notice that, as \bar{N} increases from \bar{N}_{GS} to $0.20N$, the excitation gap decreases and, in particular, it decreases faster for $J_2 = 0.48J_1$ than for $J_2 = 0.52J_1$. Indeed, the excitation gap almost vanishes as \bar{N} approaches $\bar{N}_{MAX,1}$. However, recall that, for the region $0.48J_1 \leq J_2 \leq 0.54J_1$, we should only consider solutions of the self-consistent problem (B13)-(B15) with $\bar{N} \leq \bar{N}_{MAX,2}$.

VI. CORRELATION FUNCTIONS

To further characterize the many-triplon state (47), we calculate spin-spin and dimer-dimer correlation functions and dimer order parameters. We concentrate on two model configurations, $J_2 = 0.48J_1$ and $J_2 = 0.52J_1$, since they exemplified the two distinct regions, $J_2 \leq 0.51J_1$ and $J_2 > 0.51J_1$, identified in Sec. V A. In addition to the (lowest-energy) many-triplon state (47) with $\bar{N} = \bar{N}_{GS}$, we also consider states with $\bar{N} > \bar{N}_{GS}$. Moreover, comparisons with the corresponding harmonic results for the columnar VBS state $|\text{VBS}\rangle$ are also made.

A. Spin-spin correlation functions

The spin-spin correlation functions $C_\alpha(r)$ are defined as

$$C_\alpha(r) = \langle \mathbf{S}_i \cdot \mathbf{S}_{i+r\hat{\alpha}} \rangle, \quad (48)$$

where \mathbf{S}_i is a spin-1/2 operator at the site i of the *original* square lattice and $\hat{\alpha} = \hat{x}, \hat{y}$ (recall that we set the lattice

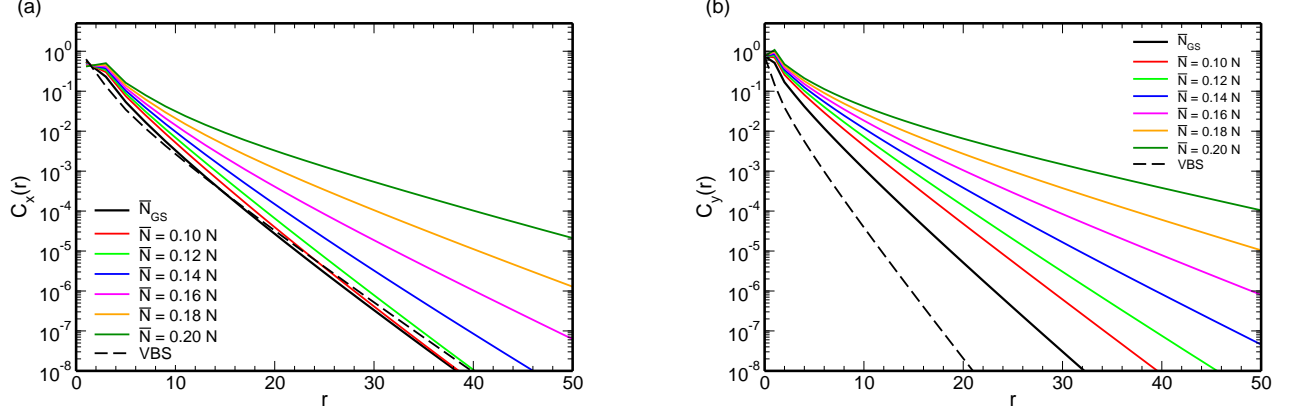


FIG. 7. Spin-spin correlation functions (odd distances r) (a) $C_x(r)$ [Eq. (49)] and (b) $C_y(r)$ [Eq. (50)] of the many-triplon state (47) for $J_2 = 0.48 J_1$. Mean-field results for different values of the triplon number \bar{N} (solid lines) are shown: $\bar{N} = \bar{N}_{GS}$ (black), $\bar{N} = 0.10 N$ (red), $\bar{N} = 0.12 N$ (green), $\bar{N} = 0.14 N$ (blue), $\bar{N} = 0.16 N$ (magenta), $\bar{N} = 0.18 N$ (orange), and $\bar{N} = 0.20 N$ (dark green). The corresponding harmonic results for the columnar VBS ground-state |VBS> are also included (dashed black line).

spacing of the original square lattice $a = 1$). In terms of the spin operators \mathbf{S}_i^1 and \mathbf{S}_i^2 of the dimerized lattice \mathcal{D} [see Fig. 1(a)], the spin-spin correlation functions (48) assume the form

$$C_x(r) = \begin{cases} \langle (\mathbf{S}_i^1)^2 \rangle, & r = 0, \\ \langle \mathbf{S}_i^1 \cdot \mathbf{S}_i^2 \rangle, & r = 1, \\ \langle \mathbf{S}_i^1 \cdot \mathbf{S}_j^1 \rangle, & r = |\mathbf{R}_j - \mathbf{R}_i| \geq 2, \\ \langle \mathbf{S}_i^1 \cdot \mathbf{S}_j^2 \rangle, & r = |\mathbf{R}_j - \mathbf{R}_i| + 1 \geq 3, \end{cases} \quad (49)$$

with $\mathbf{R}_j - \mathbf{R}_i = 2(j-i)\hat{x}$ and \mathbf{R}_i being a vector of the dimerized lattice \mathcal{D} , and

$$C_y(r) = \langle \mathbf{S}_i^1 \cdot \mathbf{S}_j^1 \rangle, \quad r = |\mathbf{R}_j - \mathbf{R}_i|, \quad (50)$$

with $\mathbf{R}_j - \mathbf{R}_i = (j-i)\hat{y}$.

It is possible to show that

$$\begin{aligned} \langle (\mathbf{S}_i^1)^2 \rangle &= \frac{3}{4}, & \langle \mathbf{S}_i^1 \cdot \mathbf{S}_i^2 \rangle &= -\frac{3}{4} (N_0 - I_{1,ii}), \\ \langle \mathbf{S}_i^1 \cdot \mathbf{S}_j^1 \rangle &= \frac{3}{2} [|I_{1,ij}|^2 - |I_{2,ij}|^2 + N_0 (I_{1,ij} + I_{2,ij})], \\ \langle \mathbf{S}_i^1 \cdot \mathbf{S}_j^2 \rangle &= \frac{3}{2} [|I_{1,ij}|^2 - |I_{2,ij}|^2 - N_0 (I_{1,ij} + I_{2,ij})], \end{aligned} \quad (51)$$

with $i \neq j$. Here, the parameter N_0 is determined within the harmonic approximation for the columnar VBS state |VBS> [Eq. (25)], as already mentioned in Sec. V A. The

integrals $I_{1,ij}$ and $I_{2,ij}$ are given by

$$\begin{aligned} I_{1,ij} &= \frac{1}{N'} \sum_{\mathbf{k}} \cos[\mathbf{k} \cdot (\mathbf{R}_i - \mathbf{R}_j)] f(\mathbf{k}), \\ I_{2,ij} &= \frac{1}{N'} \sum_{\mathbf{k}} \cos[\mathbf{k} \cdot (\mathbf{R}_i - \mathbf{R}_j)] \bar{f}(\mathbf{k}), \end{aligned} \quad (52)$$

with $N' = N/2$, and the functions $f(\mathbf{k})$ and $\bar{f}(\mathbf{k})$ being defined as

$$f(\mathbf{k}) \equiv \langle t_{\mathbf{k}\alpha}^\dagger t_{\mathbf{k}\alpha} \rangle, \quad \bar{f}(\mathbf{k}) \equiv \langle t_{\mathbf{k}\alpha}^\dagger t_{-\mathbf{k}\alpha}^\dagger \rangle. \quad (53)$$

With the aid of the Bogoliubov transformation (20), one shows that, for the columnar VBS state |VBS> within the harmonic approximation, the functions $f(\mathbf{k})$ and $\bar{f}(\mathbf{k})$ read

$$\begin{aligned} f(\mathbf{k}) &= v_{\mathbf{k}}^2 = \frac{1}{2} \left(-1 + \frac{A_{\mathbf{k}}}{\Omega_{\mathbf{k}}} \right), \\ \bar{f}(\mathbf{k}) &= -v_{\mathbf{k}} u_{\mathbf{k}} = -\frac{B_{\mathbf{k}}}{2\Omega_{\mathbf{k}}}, \end{aligned} \quad (54)$$

with $u_{\mathbf{k}}$ and $v_{\mathbf{k}}$ being the Bogoliubov coefficients (24). Similarly, using both Bogoliubov transformations (20) and (40), one finds that, for the many-triplon state (47),

$$\begin{aligned} f(\mathbf{k}) &= (u_{\mathbf{k}} \bar{v}_{\mathbf{k}} + v_{\mathbf{k}} \bar{u}_{\mathbf{k}})^2 \\ &= \frac{1}{2\omega_{\mathbf{k}} \Omega_{\mathbf{k}}} (A_{\mathbf{k}} \bar{A}_{\mathbf{k}} + B_{\mathbf{k}} \bar{B}_{\mathbf{k}} - \omega_{\mathbf{k}} \Omega_{\mathbf{k}}), \end{aligned} \quad (55)$$

$$\begin{aligned} \bar{f}(\mathbf{k}) &= -(u_{\mathbf{k}} \bar{v}_{\mathbf{k}} + v_{\mathbf{k}} \bar{u}_{\mathbf{k}}) (u_{\mathbf{k}} \bar{u}_{\mathbf{k}} + v_{\mathbf{k}} \bar{v}_{\mathbf{k}}) \\ &= -\frac{1}{2\omega_{\mathbf{k}} \Omega_{\mathbf{k}}} (A_{\mathbf{k}} \bar{B}_{\mathbf{k}} + B_{\mathbf{k}} \bar{A}_{\mathbf{k}}), \end{aligned} \quad (56)$$

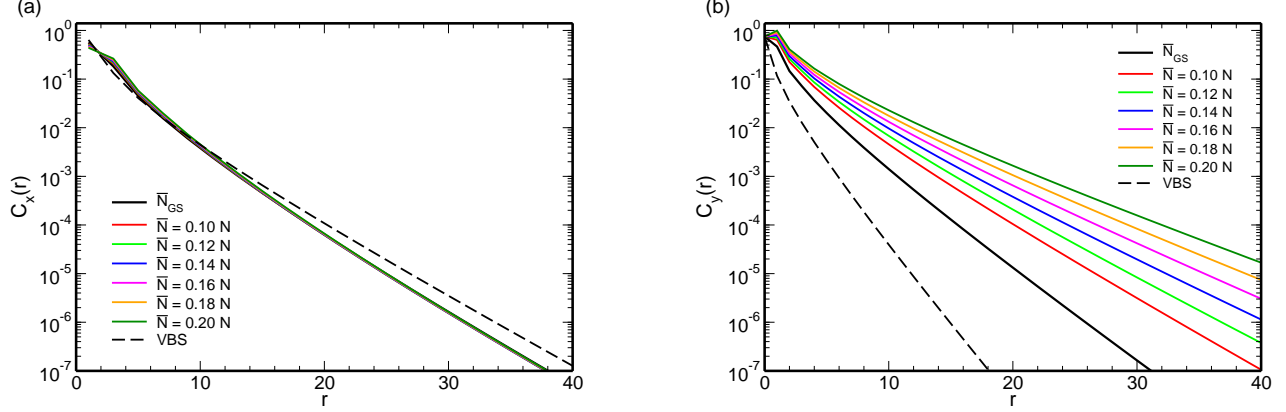


FIG. 8. Spin-spin correlation functions (odd distances r) (a) $C_x(r)$ [Eq. (49)] and (b) $C_y(r)$ [Eq. (50)] of the many-triplon state (47) for $J_2 = 0.52 J_1$. Mean-field results for different values of the triplon number \bar{N} (solid lines) are shown: $\bar{N} = \bar{N}_{GS}$ (black), $\bar{N} = 0.10 N$ (red), $\bar{N} = 0.12 N$ (green), $\bar{N} = 0.14 N$ (blue), $\bar{N} = 0.16 N$ (magenta), $\bar{N} = 0.18 N$ (orange), and $\bar{N} = 0.20 N$ (dark green). The corresponding harmonic results for the columnar VBS ground-state |VBS) are also included (dashed black line).

with $\bar{u}_{\mathbf{k}}$ and $\bar{v}_{\mathbf{k}}$ being the Bogoliubov coefficients (44).

Figure 7 shows, for $J_2 = 0.48 J_1$, the spin-spin $C_x(r)$ [Fig. 7(a)] and $C_y(r)$ [Fig. 7(b)] correlation functions of the columnar VBS ground state (dashed black lines) and of the many-triplon state (47) (solid lines) with different values of the triplon number \bar{N} . One notices that, for the columnar VBS state, both spin-spin correlation functions decay exponentially, as expected for a phase with a finite (triplet) excitation gap. Moreover, the correlation length associated with $C_x(r)$ is larger than the one related to $C_y(r)$. Such distinct behaviours found for the $C_x(r)$ and the $C_y(r)$ correlation functions are related to the symmetries of the columnar VBS state: recall that we consider, in particular, a columnar VBS state with dimers along the x direction. Similarly, for the many-triplon state, the two spin-spin correlation functions also decay exponentially, regardless the triplon number \bar{N} . For the columnar VBS ground state and the many-triplon states with $\bar{N} \leq 0.12 N$, the correlation lengths associated with the correlation function $C_x(r)$ are approximately equal while, for $\bar{N} \geq 0.14 N$, the correlation length increases with \bar{N} . Such features might be related to the fact that the excitation gap above the columnar VBS ground state and the ones above the many-triplon state with $\bar{N}_{GS} \leq \bar{N} \leq 0.10 N$ are approximately equal [see Fig. 4(a)] while, for $\bar{N} > 0.10 N$, the excitation gap above the many-triplon state decreases as \bar{N} increases. On the other hand, for $\bar{N} < 0.14 N$, the correlation length associated with the correlation function $C_y(r)$ seems to be less sensitive to the excitation gap, since it always increases with the triplon number \bar{N} . Again, these different features displayed by the $C_x(r)$ and the $C_y(r)$ correlation functions of the many-triplon state with $\bar{N} < 0.14 N$ might be due to the symmetries of the columnar VBS

(reference) state. Interesting, for larger values of the triplon number \bar{N} , the behaviour of the $C_x(r)$ and the $C_y(r)$ correlation functions are quite similar, indicating that, in this case, the many-triplon states should display a more homogeneous singlet pattern than the columnar VBS ground state.

The spin-spin $C_x(r)$ and $C_y(r)$ correlation functions of the columnar VBS ground state and the many-triplon state (47) with different values of the triplon number \bar{N} for $J_2 = 0.52 J_1$ are shown in Figs. 8(a) and (b), respectively. Similar to the configuration $J_2 = 0.48 J_1$, both correlation functions exponentially decay with the distance r . Interesting, for the many-triplon state, the correlation lengths associated with the correlation function $C_x(r)$ are independent of the triplon number \bar{N} and they are almost equal to the corresponding one of the columnar VBS ground state. Again, this feature might be related to the fact that the excitation gap above the many-triplon state slowly decreases with the triplon number \bar{N} and they are close to the excitation gap above the columnar VBS ground state [see Fig. 4(b)]. On the other hand, the correlation length associated with the correlation function $C_y(r)$ increases with \bar{N} , similar to the behaviour found for $J_2 = 0.48 J_1$. Differently from the configuration $J_2 = 0.48 J_1$, here the behaviour of the $C_x(r)$ and the $C_y(r)$ correlation functions do not indicate that the many-triplon states with large \bar{N} are constituted by a more homogeneous singlet pattern than the corresponding columnar VBS state.

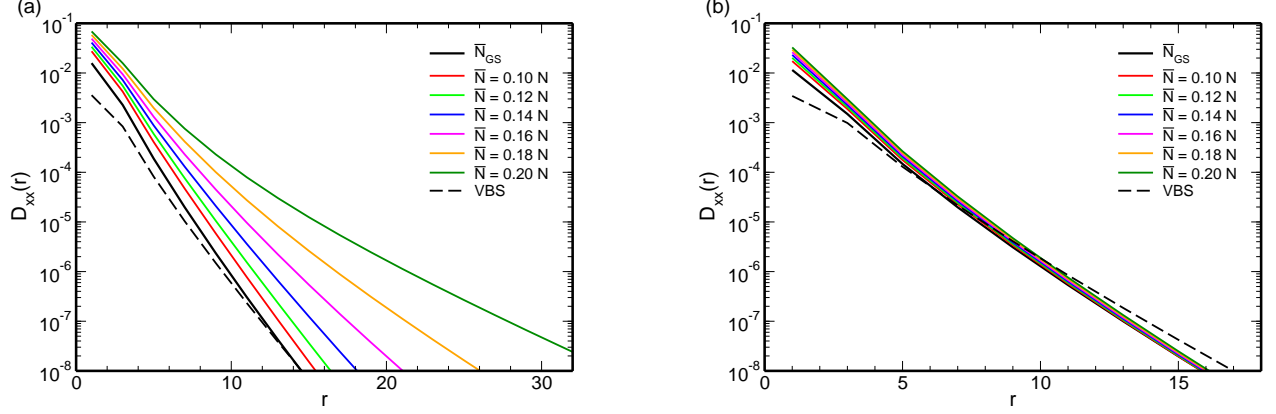


FIG. 9. Dimer-dimer correlation function (odd distances r) $D_{xx}(r)$ [Eq. (59)] of the many-triplon state (47) for (a) $J_2 = 0.48 J_1$ and (b) $J_2 = 0.52 J_1$. Mean-field results for different values of the triplon number \bar{N} (solid lines) are shown: $\bar{N} = \bar{N}_{GS}$ (black), $\bar{N} = 0.10 N$ (red), $\bar{N} = 0.12 N$ (green), $\bar{N} = 0.14 N$ (blue), $\bar{N} = 0.16 N$ (magenta), $\bar{N} = 0.18 N$ (orange), and $\bar{N} = 0.20 N$ (dark green). The corresponding harmonic results for the columnar VBS ground-state |VBS> are also included (dashed black line).

B. Dimer-dimer correlation functions

The dimer-dimer correlation functions $D_{\alpha\beta}(i, j)$ are defined as

$$D_{\alpha\beta}(i, j) = \langle B_\alpha(i) B_\beta(j) \rangle - \langle B_\alpha(i) \rangle \langle B_\beta(j) \rangle, \quad (57)$$

where the dimer operator $B_\alpha(i)$ reads

$$B_\alpha(i) = \mathbf{S}_i \cdot \mathbf{S}_{i+\hat{\alpha}}, \quad (58)$$

with \mathbf{S}_i being a spin-1/2 operator at the site i of the original square lattice and $\hat{\alpha} = \hat{x}, \hat{y}$. Similar to the spin-spin correlation functions (48), we rewrite the dimer-dimer correlation functions (57) in terms of the spin operators \mathbf{S}_i^1 and \mathbf{S}_i^2 of the dimerized lattice \mathcal{D} . In particular, the dimer-dimer correlation function $D_{xx}(r)$ assumes the form

$$D_{xx}(r) = \langle (\mathbf{S}_i^1 \cdot \mathbf{S}_i^2) (\mathbf{S}_l^2 \cdot \mathbf{S}_j^1) \rangle - \langle (\mathbf{S}_i^1 \cdot \mathbf{S}_i^2) \rangle \langle (\mathbf{S}_l^2 \cdot \mathbf{S}_j^1) \rangle, \quad (59)$$

for $r = |\mathbf{R}_j - \mathbf{R}_i| - 1$, and

$$D_{xx}(r) = \langle (\mathbf{S}_i^1 \cdot \mathbf{S}_i^2) (\mathbf{S}_j^1 \cdot \mathbf{S}_j^2) \rangle - \langle (\mathbf{S}_i^1 \cdot \mathbf{S}_i^2) \rangle \langle (\mathbf{S}_j^1 \cdot \mathbf{S}_j^2) \rangle, \quad (60)$$

for $r = |\mathbf{R}_j - \mathbf{R}_i|$, with $\mathbf{R}_j - \mathbf{R}_i = 2(j-i)\hat{x}$, $\mathbf{R}_j - \mathbf{R}_l = 2\hat{x}$, and \mathbf{R}_i being a vector of the dimerized lattice \mathcal{D} . Here, it is also possible to express $D_{xx}(r)$ in terms of the integrals (52):

$$D_{xx}(r) = -\frac{3}{8} N_0 (I_{1,ij} + I_{2,ij}) (I_{1,il} + I_{2,il}) + \frac{3}{4} I_{1,jl} (I_{1,ij} I_{1,li} + I_{2,ij} I_{2,li}) - \frac{3}{4} I_{2,jl} (I_{1,ij} I_{2,li} + I_{2,ij} I_{1,li}), \quad (61)$$

for $r = |\mathbf{R}_j - \mathbf{R}_i| - 1$, and

$$D_{xx}(r) = \frac{3}{16} [|I_{1,ij}|^2 + |I_{2,ij}|^2], \quad (62)$$

for $r = |\mathbf{R}_j - \mathbf{R}_i|$, with the parameter N_0 being determined within the harmonic approximation for the columnar VBS state, see Eq. (25). Therefore, with the aid of Eqs. (52)–(56), we can determine the dimer-dimer correlation function $D_{xx}(r)$ of the columnar VBS state and the many-triplon state (47).

The dimer-dimer correlation function $D_{xx}(r)$ of the columnar VBS ground state and of the many-triplon state (47) with different values of the triplon number \bar{N} for $J_2 = 0.48 J_1$ are shown in Fig. 9(a). Similar to the columnar VBS state, the dimer-dimer correlation function of the many-triplon states decay exponentially, regardless the value of the triplon number \bar{N} . Such a behaviour indicates that the singlet excitation gap above the many-triplon state is finite. Moreover, the correlation length associated with $D_{xx}(r)$ increases with the triplon number \bar{N} . These features are quite similar to the ones found for the spin-spin correlation function $C_x(r)$ [Fig. 7(a)], although the dimer correlation decays faster than the corresponding spin one and the dimer correlation length always increases with the triplon number \bar{N} , even for $\bar{N} \leq 0.12 N$.

For $J_2 = 0.52 J_1$, we also found that the correlation function $D_{xx}(r)$ of both columnar VBS ground state and many-triplon states decay exponentially, see Fig. 9(b). Differently from the configuration $J_2 = 0.48 J_1$, here the correlation length associated with $D_{xx}(r)$ is independent of the triplon number \bar{N} and it is close to the correlation length of the columnar VBS state. Again, these features are quite similar to the ones found for the corresponding spin-spin correlation function $C_x(r)$ [Fig. 8(a)], apart

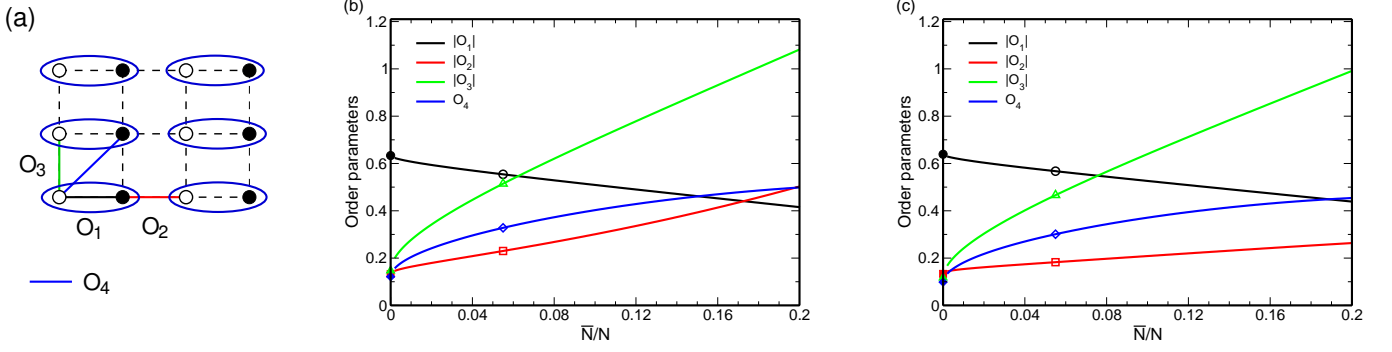


FIG. 10. (a) Schematic representation of the dimer order parameters (63) for the square lattice. Dimer order parameters (63) of the many-triplon state (47) as a function of the ratio \bar{N}/N for (b) $J_2 = 0.48 J_1$ and (c) $J_2 = 0.52 J_1$. The solid symbols are the harmonic results for the columnar VBS ground state while the open symbols are the mean-field results for the (lowest-energy) many-triplon state (47) with $\bar{N} = \bar{N}_{GS}$.

from the fact that the dimer correlations decay faster than the corresponding spin ones.

C. Dimer order parameters

Let us now consider the following dimer order parameters:

$$\begin{aligned}
 O_1 &= \langle \mathbf{S}_i^1 \cdot \mathbf{S}_i^2 \rangle, \\
 O_2 &= \langle \mathbf{S}_i^2 \cdot \mathbf{S}_j^1 \rangle, \quad \mathbf{R}_j - \mathbf{R}_i = 2a\hat{x}, \\
 O_3 &= \langle \mathbf{S}_i^1 \cdot \mathbf{S}_j^1 \rangle, \quad \mathbf{R}_j - \mathbf{R}_i = a\hat{y}, \\
 O_4 &= \langle \mathbf{S}_i^1 \cdot \mathbf{S}_j^2 \rangle, \quad \mathbf{R}_j - \mathbf{R}_i = a\hat{y}, \quad (63)
 \end{aligned}$$

where \mathbf{S}_i^1 and \mathbf{S}_i^2 are spin operators at the site i of the dimerized lattice \mathcal{D} and \mathbf{R}_i is the vector associated with the site i . The four dimer order parameters O_i are illustrated in Fig. 10(a). With the aid of Eq. (51), one sees that the dimer order parameters (63) can be written in terms of the integrals $I_{1,ij}$ and $I_{2,ij}$ [Eq. (52)], and therefore, they can be easily calculated for both columnar VBS state and many-triplon state (47).

Figure 10 shows the behaviour of the dimer order parameters (63) as a function of the triplon number \bar{N} for $J_2 = 0.48 J_1$ [Fig. 10(b)] and $J_2 = 0.52 J_1$ [Fig. 10(c)]. The results for the columnar VBS ground state are indicated by the solid symbols, while the results for the (lowest-energy) many-triplon state with $\bar{N} = \bar{N}_{GS}$ are indicated by the open ones. As expected, for the columnar VBS ground state, we found that $|O_1| > |O_2| \approx |O_3| \approx |O_4|$ while, for the lowest-energy many-triplon state with $\bar{N} = \bar{N}_{GS}$, we have $|O_1| \approx |O_3| > |O_2| \approx |O_4|$, i.e., apart from the value of the dimer order parameter O_3 (see discussion below), such a state might display the same features of the columnar VBS state. For a

large triplon number \bar{N} , in particular, $\bar{N} \sim 0.17$, we notice that, $|O_1| \approx |O_2| \approx |O_4| \sim 0.46$ for $J_2 = 0.48 J_1$, while $|O_1| \approx |O_4| \sim 0.45 > |O_2|$ for $J_2 = 0.52 J_1$. Therefore, the dimer order parameters indicate that the many-triplon states with large \bar{N} might display a more homogeneous singlet pattern for $J_2 = 0.48 J_1$ than for $J_2 = 0.52 J_1$. Recall that such features are in agreement with the ones found for the spin-spin $C_x(r)$ and $C_y(x)$ correlation functions, see Sec. VIA.

Finally, concerning the behaviour of the dimer order parameter O_3 with the triplon number \bar{N} , it is not clear, at the moment, the reason O_3 increases so fast with \bar{N} . We believe it could be an artefact of the approximations involved in our mean-field calculations. Indeed, such an artefact could also affect the behaviour of the spin-spin correlation function $C_y(r)$: recall that the correlation length associated with $C_y(r)$ seems to be less sensitive to the excitation gap than the correlation length related to the correlation function $C_x(r)$, see Sec. VIA.

VII. ENTANGLEMENT ENTROPY

In this section, we calculate the bipartite von Neumann entanglement entropy \mathcal{S} of the columnar VBS and the many-triplon states. In particular, we follow the procedure [23], that was recently employed to calculate the entanglement entropies of the ground state of spin-1/2 dimerized Heisenberg AFMs on a square lattice.

The bipartite entanglement entropy of the ground state $|\Psi\rangle$ of a system S is defined, for instance, as the von Neumann entropy [41, 42],

$$\mathcal{S} = \mathcal{S}(\rho_A) = -\text{Tr}(\rho_A \ln \rho_A), \quad (64)$$

where A is a subsystem (arbitrary size and shape), \bar{A} is its complementary such that the system $S = A \cup \bar{A}$, and $\rho_A = \text{Tr}_{\bar{A}}|\Psi\rangle\langle\Psi|$ is the reduced density matrix of the subsystem A . For a generic quadratic Hamiltonian

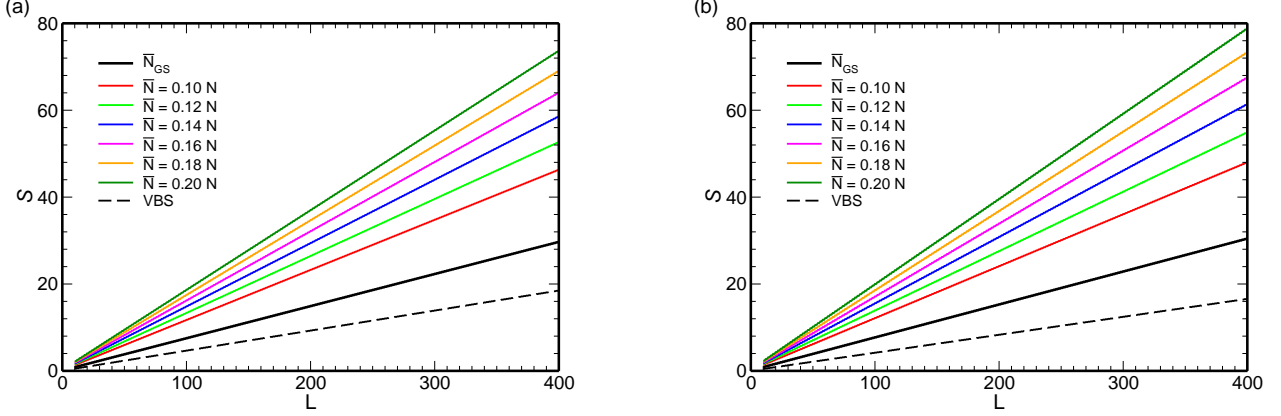


FIG. 11. The von Neumann entanglement entropy \mathcal{S} as a function of the size L of the (line) subsystem A of the many-triplon state (47) for (a) $J_2 = 0.48 J_1$ and (b) $J_2 = 0.52 J_1$. Results for different values of the triplon number \tilde{N} (solid lines) are shown: $\tilde{N} = \tilde{N}_{GS}$ (black), $\tilde{N} = 0.10 N$ (red), $\tilde{N} = 0.12 N$ (green), $\tilde{N} = 0.14 N$ (blue), $\tilde{N} = 0.16 N$ (magenta), $\tilde{N} = 0.18 N$ (orange), and $\tilde{N} = 0.20 N$ (dark green). The corresponding harmonic results for the columnar VBS ground-state [VBS] are also included (dashed black line).

written in terms of boson operators, it is possible to show that the entanglement entropy (64) assumes the form

$$\mathcal{S} = \sum_{m=1}^{N_A} \sum_{\epsilon=\pm 1} \epsilon \left(\frac{\mu_m + \epsilon}{2} \right) \ln \left(\frac{\mu_m + \epsilon}{2} \right), \quad (65)$$

where μ_m^2 are the eigenvalues of the so-called correlation matrix C (for the definition, see Eq. (41) of Ref. [23]) and $N_A < N$ is the number of sites of the subsystem A . In particular, for a one-dimensional (line) subsystem A [a spin chain of size L , see Fig. 1(b)], the eigenvalues μ_m^2 of the correlation matrix can be analytically calculated. For the columnar VBS ground state described by the harmonic Hamiltonian (19), we have

$$\mu_m^2 = \left(\frac{1}{N_y} \sum_{k_y} \frac{A_{m,k_y}}{\omega_{m,k_y}} \right)^2 - \left(\frac{1}{N_y} \sum_{k_y} \frac{B_{m,k_y}}{\omega_{m,k_y}} \right)^2, \quad (66)$$

where the index $m = 1, 2, \dots$ and N_A is related to the momentum k_x parallel to the system-subsystem boundary,

$$k_x = -\frac{\pi}{2} + \frac{2\pi(m-1)}{L+2}, \quad (67)$$

with $N' = N_A N_y$ and $N_A = (L+2)/2$. Moreover, $A_{\mathbf{k}}$ [Eq. (15)] and $B_{\mathbf{k}}$ [Eq. (16)] are the coefficients of the harmonic Hamiltonian (19), and $\omega_{\mathbf{k}}$ is the energy of the triplons (23). Similarly, for the many-triplon state (47) described by the mean-field Hamiltonian (37), the eigenvalues of the correlation matrix are also given by Eq. (66), but with the replacements: $A_{\mathbf{k}} \rightarrow \tilde{A}_{\mathbf{k}}$, $B_{\mathbf{k}} \rightarrow \tilde{B}_{\mathbf{k}}$ [Eq. (38)], and $\omega_{\mathbf{k}} \rightarrow \tilde{\Omega}_{\mathbf{k}}$ [Eq. (43)].

The bipartite von Neumann entanglement entropy \mathcal{S} in terms of the subsystem size L of the columnar VBS ground state and the many-triplon state with different values of the triplon number \tilde{N} for $J_2 = 0.48 J_1$ and $J_2 = 0.52 J_1$ are shown in Figs. 11(a) and (b), respectively. As expected for a two-dimensional gapped phase [43], we find that the entanglement entropy is dominated by an area law for both columnar VBS and many-triplon states: we fit the data shown in Figs. 11(a) and (b) with the curve

$$\mathcal{S} = aL + b \ln L + c, \quad (68)$$

and find that the coefficient $b < 10^{-5}$, see Table I for details. Moreover, for a given subsystem size L , we notice that the entanglement entropy increases as the triplon number \tilde{N} increases. Such a feature is similar to the one found for the square lattice dimerized Heisenberg AFMs (see Figs. 6(a) and (b) of Ref. [23]): as the dimerization decreases and the system approaches the Néel-VBS quantum phase transition, the number of triplets t increases, and therefore, the entanglement entropy increases although it seems not to diverge at the quantum critical point.

VIII. SUMMARY AND DISCUSSION

The bond-operator representation for spin operators introduced by Sachdev and Bhatt [19] is an interesting formalism that allows us to analytically describe a VBS phase of a Heisenberg model. Not only dimerized VBS phases (as the columnar VBS one discussed in this paper) could be described within this formalism, but it could also be employed to study VBS phases with larger unit

cells, such as the tetramerized plaquette VBS [22, 32]. Indeed, the bond-operator formalism is quite suitable for the description of a VBS phase: In this case, it is possible to identify a singlet pattern (reference state) and label the different spins that constituted each singlet (unit cell); although each spin within the unit cell has a distinct representation in terms of the bosonic bond operators [see, e.g., Eq. (4)], the mapping from a spin Hamiltonian to an effective boson one is well defined, since the singlets are regularly distributed in space.

It would be interesting to apply the bond-operator formalism to describe the another set of quantum paramagnetic phases, the spin liquids. It would be an alternative to the Schwinger boson formalism [20] that is usually employed to analytically study spin-liquid phases [39]. However, such an application is rather difficult to implement: in this case, it is not possible to define an initial singlet pattern (reference state), and therefore, a mapping from a Heisenberg model to an effective boson one is not well-defined. In contrast, in the Schwinger boson formalism, all spin operators have the same expansion in terms of the boson operators, and therefore, a mapping from a spin model to a boson one can be done without a reference state (the initial singlet pattern). As mentioned in Sec. I, one motivation to study a system within a fixed number of triplons b above a VBS ground state is to check whether the possible many-triplon state could restore the lattice symmetries broken when the VBS phase sets in. In principle, such a many-triplon state could describe a spin-liquid state.

For the square lattice spin-1/2 J_1 - J_2 AFM Heisenberg model with the columnar VBS as a reference state, our mean-field results indicate that the many-triplon state (47) is stable, although the lowest-energy one has a quite small number of triplons $\bar{N} = \bar{N}_{GS}$ [see Fig. 6]. Therefore, we would expect that the columnar VBS ground state and the many-triplon state with $\bar{N} = \bar{N}_{GS}$ would have similar features. Indeed, for $J_2 = 0.48J_1$ and $J_2 = 0.52J_1$, we found that the spin-spin $C_x(r)$ [Figs. 7(a) and 8(a)] and the dimer-dimer $D_{xx}(r)$ [Fig. 9] correlation functions of both states decay exponentially with

correlation lengths approximately equal. Such features are related to the fact that the excitation gap of both states are quite close [see Fig 5]. On the other hand, the correlation length associated with the spin-spin correlation function $C_y(r)$ of the columnar VBS state is smaller than the one of the lowest-energy many-triplon state [see Figs. 7(b) and 8(b)]. Moreover, although the excitation gap above the two states are approximately equal, the corresponding excitation spectra are indeed distinct, as exemplified for $J_2 = 0.48J_1$ [Fig. 4(a)] and $J_2 = 0.52J_1$ [Fig. 4(b)]. In particular, the momenta associated with the excitation gap are equal for both columnar VBS and lowest-energy many-triplon states only for $J_2 \leq 0.51J_1$.

In addition to the lowest-energy many-triplon state with $\bar{N} = \bar{N}_{GS}$, we also study (high energy) many-triplon states with $\bar{N} > \bar{N}_{GS}$. For $J_2 = 0.48J_1$ and $J_2 = 0.52J_1$, we found that the excitation gaps are finite, they decrease with the triplon number \bar{N} , and they are located at the Y ($J_2 = 0.48J_1$) and M ($J_2 = 0.48J_1$) points of the first Brillouin zone [Fig. 4]. Moreover, we also found that the spin-spin [Figs. 7 and 8] and the dimer-dimer [Fig. 9] correlation functions of the many-triplon states decay exponentially, regardless the triplon number \bar{N} . In fact, the behaviour of the spin-spin correlation functions indicates that, only for $J_2 = 0.48J_1$, the many-triplon states with large triplon number \bar{N} might display a more homogeneous singlet pattern than the columnar VBS state. Interesting, recent DMRG calculations also found distinct features for the model parameters $J_2 = 0.48J_1$ and $J_2 = 0.52J_1$: Gong *et al.* [33] found evidences for a gapless phase for $0.44J_1 < J_2 < 0.50J_1$ and a plaquette VBS ground state for $0.50J_1 < J_2 < 0.61J_1$; the calculations of Wang and Sandvik [36] indicated that a gapless spin-liquid phase sets in for $0.46J_1 < J_2 < 0.52J_1$ while a (columnar) VBS ground state, for $0.52J_1 < J_2 < 0.62J_1$. Although a proper comparison between our results and the DMRG ones is rather difficult, our procedure seems to be able to distinguish the parameter regions $J_2 \lesssim 0.51J_1$ and $J_2 \gtrsim 0.51J_1$ of the square lattice J_1 - J_2 model.

Monte Carlo simulations were employed to calculate the spin-spin and the dimer-dimer correlation functions of the (nearest-neighbor) resonating-valence-bond (RVB) state on the square lattice [44, 45]. It was found that the spin correlations decay exponentially while the dimer ones decay algebraically with an exponent $\alpha \sim 1.2$. Such a behaviour is similar to the classical dimer model, although the dimer correlations of the RVB state decay more slowly than the ones of the classical dimer model ($\alpha = 2.0$). Interesting, Monte Carlo calculations for the nearest-neighbor RVB state but on the triangular and kagome lattices [46, 47] and for a RVB state on the square lattice whose longest valence bonds are between next-nearest-neighbors [47] found that both spin and dimer correlations decay exponentially. Comparing with our mean-field results for the many-triplon state (47), one sees that it displays the same features of the next-nearest-neighbor RVB state on the square lattice. Since the spin correlations for $J_2 = 0.48J_1$ also indicate

TABLE I. Coefficients a , b , and c obtained by fitting the von Neumann entanglement entropies \mathcal{S} shown in Figs. 11(a) and (b) with the curve (68).

\bar{N}	$J_2 = 0.48 J_1$			$J_2 = 0.52 J_1$		
	a	b	c	a	b	c
VBS	0.05	1.82e-05	0.05	0.04	1.18e-08	0.04
\bar{N}_{GS}	0.07	4.28e-05	0.12	0.08	4.05e-05	0.12
0.10	0.11	7.51e-07	0.18	0.12	2.14e-08	0.18
0.12	0.13	8.17e-09	0.21	0.14	6.64e-09	0.21
0.14	0.15	5.93e-09	0.23	0.15	5.16e-09	0.23
0.16	0.16	5.03e-09	0.25	0.17	4.69e-09	0.25
0.18	0.17	5.02e-09	0.27	0.18	5.19e-09	0.27
0.20	0.18	4.79e-09	0.28	0.19	4.49e-09	0.29

that the many-triplon states with large \bar{N} may be characterized by a more homogeneous singlet pattern than the columnar VBS ground state, we would expect that, in this case, the many-triplon state could describe a spin-liquid phase.

To further characterize the many-triplon states with large \bar{N} , we determined the behaviour of the dimer order parameters (63) with the triplon number \bar{N} [Fig. 10]. For $J_2 = 0.48J_1$, we found that the dimer order parameters seem not to converge to the same value as \bar{N} increases, although $|O_1| \approx |O_2| \approx |O_4| \sim 0.46$ when $\bar{N} \sim 0.17$. Such a behaviour of the dimer order parameters indicates that the many-triplon states with large \bar{N} do not correspond to a spin-liquid state: In a spin-liquid phase, the dimer order parameters are approximately equal, as found, e.g., for the nearest-neighbor RVB state on the kagome lattice in Ref. [46]; for the many-triplon state, we would expect that a transition from a columnar VBS state to spin-liquid one as \bar{N} increases may be signaled by a convergence of the dimer order parameters to a single value, i.e., $|O_1| \sim |O_2| \sim |O_3| \sim |O_4|$ for $\bar{N} > \bar{N}_c$, a feature that is not observed.

Finally, we also calculated the bipartite von Neumann entanglement entropy of the columnar VBS and many-triplon states [Fig. 11]. Fitting the data with the curve (68), we found that the entanglement entropies obey an area law, as expected for a two-dimensional gapped phase, and that the coefficient $c > 0$ and it increases with the triplon number \bar{N} for both $J_2 = 0.48J_1$ and $J_2 = 0.52J_1$. These results corroborate the fact that the many-triplon state with large \bar{N} do not describe a spin-liquid state, in particular, a gapped Z_2 spin liquid: In this case, the entanglement entropy obeys an area law with $c = -\gamma = -\ln 2$, where γ is the topological entanglement entropy [11]; such feature is found, e.g., for the nearest-neighbor RVB state on the kagome and triangular lattices [48]; again, for the many-triplon state, a transition from a VBS state to a spin-liquid one with the triplon number \bar{N} would be characterized by $c \rightarrow -\ln 2$.

In summary, we have studied a system of interacting triplons b , the elementary excitations above a VBS ground state, described by an effective boson model derived within the bond-operator formalism. In particular, we chose the spin-1/2 J_1 - J_2 AFM Heisenberg model on a square lattice and focused on the possible columnar VBS ground state. We found that a many-triplon state is stable, but the lowest-energy one is constituted by a small number of triplons. Moreover, we also discussed the properties of many-triplon states constituted by large number of triplons. In particular, the spin-spin correlation functions indicated that such states might be characterized by a more homogeneous singlet pattern than the columnar VBS ground state. However, based on the mean-field results for the dimer order parameters and the bipartite entanglement entropy, we concluded that the many-triplon states with large triplon number \bar{N} may not describe a (gapped) spin-liquid phase.

It is important to emphasize that our conclusions

about the nature of the many-triplon states, in particular, the ones with large triplon number \bar{N} , are related to a particular Heisenberg model and VBS (reference) state. As mentioned in Sec. III, it is not clear, at the moment, whether the ground state of the J_1 - J_2 model within the intermediate parameter region $0.4J_1 \lesssim J_2 \lesssim 0.6J_1$ is a VBS or a spin-liquid state. It would be interesting to apply the mean-field procedure discussed here to a Heisenberg model for which there are (strong) evidences for a gapped spin-liquid phase, contrast the obtained results with the ones derived here, and, in particular, to check whether the (possible) lowest-energy many-triplon state is constituted by a large number of triplons. A possible candidate is the spin-1/2 J_1 - J_2 AFM Heisenberg model on a *triangular* lattice: although a more recent DMRG calculation pointed to a gapless spin-liquid phase [49], previous DMRG simulations [50–52] indicated that a gapped spin-liquid ground state may set in within the intermediate parameter region $0.07J_1 \lesssim J_2 \lesssim 0.15J_1$.

ACKNOWLEDGMENTS

We thank A. O. Caldeira, E. Miranda, L. Leite, and M. Vojta for helpful discussions and FAPESP, Project No. 2010/00479-6, for the partial financial support.

Appendix A: Effective boson model I in real space

In this section, we quote the expression of the effective boson model (8) in terms of the singlet s_i and triplet $t_{i\alpha}$ boson operators.

Substituting the (generalized) bond operator representation (4) into the Heisenberg model (6), it is possible to show that the four terms of the Hamiltonian (8) read

$$\begin{aligned} \mathcal{H}_0 &= -\frac{3}{4}J_1 \sum_i s_i^\dagger s_i, \\ \mathcal{H}_2 &= \frac{J_1}{4} \sum_i t_{i\alpha}^\dagger t_{i\alpha} + \frac{1}{4} \sum_{i,\tau} \zeta_2(\tau) \left(s_i s_{i+\tau}^\dagger t_{i\alpha}^\dagger t_{i+\tau\alpha} + \text{H.c.} \right. \\ &\quad \left. + s_i^\dagger s_{i+\tau}^\dagger t_{i\alpha} t_{i+\tau\alpha} + \text{H.c.} \right), \\ \mathcal{H}_3 &= \frac{i}{4} \epsilon_{\alpha\beta\lambda} \sum_{i,\tau} \zeta_3(\tau) \left[\left(s_i^\dagger t_{i\alpha} + t_{i\alpha}^\dagger s_i \right) t_{i+\tau\beta}^\dagger t_{i+\tau\lambda} \right. \\ &\quad \left. - (i \leftrightarrow i + \tau) \right], \\ \mathcal{H}_4 &= -\frac{1}{4} \epsilon_{\alpha\beta\lambda} \epsilon_{\alpha\mu\nu} \sum_{i,\tau} \zeta_4(\tau) t_{i\beta}^\dagger t_{i+\tau\mu}^\dagger t_{i\lambda} t_{i+\tau\nu}, \end{aligned} \quad (\text{A1})$$

where the summation convention over repeated indices is implied and the $\zeta_i(\tau)$ functions are defined as

$$\begin{aligned} \zeta_2(\tau) &= 2(J_1 - J_2)\delta_{\tau,2} - J_1\delta_{\tau,1} - J_2(\delta_{\tau,1+2} + \delta_{\tau,1-2}), \\ \zeta_3(\tau) &= J_1\delta_{\tau,1} + J_2(\delta_{\tau,1+2} + \delta_{\tau,1-2}), \\ \zeta_4(\tau) &= 2(J_1 + J_2)\delta_{\tau,2} + J_1\delta_{\tau,1} + J_2(\delta_{\tau,1+2} + \delta_{\tau,1-2}), \end{aligned}$$

with τ_n being the dimer nearest-neighbor vectors (7).

Appendix B: Details: effective boson model II and the mean-field approximation for a system of \bar{N} triplons

In this section, we quote alternative expressions for the constant E_{40} [Eq. (29)], the coefficients $A_{\mathbf{k}}^{(4)}$ and $B_{\mathbf{k}}^{(4)}$ [Eq. (32)] of the quadratic term \mathcal{H}_{24} [Eq. (30)], the expressions of the coefficients of the mean-field Hamiltonian (35), in addition to provide some details of the self-consistent problem related to the mean-field approximation discussed in Sec. V A.

We start considering the constant E_{40} and the quadratic term \mathcal{H}_{24} . Since the bare quartic vertex (18) can be written as

$$\gamma_{\mathbf{k}-\mathbf{p}} = -\frac{1}{2} \sum_{i=1}^4 C_i [f_i(\mathbf{k})f_i(\mathbf{p}) + \bar{f}_i(\mathbf{k})\bar{f}_i(\mathbf{p})], \quad (\text{B1})$$

where the coefficients C_i are defined as

$$C_1 = J_1, \quad C_2 = 2(J_1 + J_2), \quad C_3 = C_4 = J_2, \quad (\text{B2})$$

the functions $f_i(\mathbf{q})$ are given by

$$f_1(\mathbf{p}) = \cos(2p_x), \quad f_2(\mathbf{p}) = \cos p_y, \quad (\text{B3})$$

$$f_3(\mathbf{p}) = \cos(2p_x + p_y), \quad f_4(\mathbf{p}) = \cos(2p_x - p_y),$$

and the functions $\bar{f}_i(\mathbf{p}) = f_i(\mathbf{p})$ with the replacement $\cos(x) \rightarrow \sin(x)$, it is interesting to define the following set of coefficients

$$a_i(i, j) = \frac{1}{N'} \sum_{\mathbf{p}} f_i(\mathbf{p})g_i(\mathbf{p}), \quad (\text{B4})$$

where $i, j = 1, 2, 3, 4$ and the functions $g_i(\mathbf{p})$ are defined in terms of the Bogoliubov coefficients (24), i.e.,

$$g_1(\mathbf{p}) = v_{\mathbf{p}}^2 = \frac{1}{2} \left(-1 + \frac{A_{\mathbf{p}}}{\omega_{\mathbf{p}}} \right), \quad g_2(\mathbf{p}) = u_{\mathbf{p}}v_{\mathbf{p}} = \frac{B_{\mathbf{p}}}{2\omega_{\mathbf{p}}}. \quad (\text{B5})$$

It is then possible to rewrite the constant E_{40} [Eq. (29)] and the coefficients $A_{\mathbf{k}}^{(4)}$ and $B_{\mathbf{k}}^{(4)}$ [Eq. (32)] as

$$E_{40} = \frac{3}{4}N \sum_{i=1}^4 C_i [a_4^2(i, 1) - a_4^2(i, 2)],$$

$$A_{\mathbf{k}}^{(4)} = \sum_{i=1}^4 C_i \frac{f_i(\mathbf{k})}{\omega_{\mathbf{k}}} [a_4(i, 1)A_{\mathbf{k}} - a_4(i, 2)B_{\mathbf{k}}], \quad B_{\mathbf{k}}^{(4)} = \sum_{i=1}^4 C_i \frac{f_i(\mathbf{k})}{\omega_{\mathbf{k}}} [a_4(i, 2)A_{\mathbf{k}} - a_4(i, 1)B_{\mathbf{k}}], \quad (\text{B6})$$

where the coefficients $A_{\mathbf{k}}$ and $B_{\mathbf{k}}$ are respectively given by Eqs. (15) and (16) and $\omega_{\mathbf{k}}$ is the triplon energy (23).

Within a mean-field approximation, that takes into account both normal $h_{\mathbf{k}}$ and anomalous $\bar{h}_{\mathbf{k}}$ expectation values (45), one shows, after a long but straightforward algebra, that the quartic term \mathcal{H}_{44} [Eq. (31)] assumes the form (35), where the constant E_{44} and the coefficients $\Delta_{1,\mathbf{k}}$ and $\Delta_{2,\mathbf{k}}$ read

$$E_{44} = \frac{3}{N'} \sum_{\mathbf{k}, \mathbf{p}} \gamma_{\mathbf{k}-\mathbf{p}} [(2u_{\mathbf{k}}v_{\mathbf{k}})(2u_{\mathbf{p}}v_{\mathbf{p}}) - (u_{\mathbf{k}}^2 + v_{\mathbf{k}}^2)(u_{\mathbf{p}}^2 + v_{\mathbf{p}}^2)] \bar{h}_{\mathbf{k}}\bar{h}_{\mathbf{p}} \\ + 2\gamma_{\mathbf{k}-\mathbf{p}} [(u_{\mathbf{k}}^2 + v_{\mathbf{k}}^2)(2u_{\mathbf{p}}v_{\mathbf{p}}) - (2u_{\mathbf{k}}v_{\mathbf{k}})(u_{\mathbf{p}}^2 + v_{\mathbf{p}}^2)] \bar{h}_{\mathbf{k}}h_{\mathbf{p}} + \gamma_{\mathbf{k}-\mathbf{p}} [(u_{\mathbf{k}}^2 + v_{\mathbf{k}}^2)(u_{\mathbf{p}}^2 + v_{\mathbf{p}}^2) - (2u_{\mathbf{k}}v_{\mathbf{k}})(2u_{\mathbf{p}}v_{\mathbf{p}})] h_{\mathbf{k}}h_{\mathbf{p}}, \quad (\text{B7})$$

$$\Delta_{1,\mathbf{k}} = -\frac{2}{N'} \sum_{\mathbf{p}} \gamma_{\mathbf{k}-\mathbf{p}} [(2u_{\mathbf{k}}v_{\mathbf{k}})(u_{\mathbf{p}}^2 + v_{\mathbf{p}}^2) - (u_{\mathbf{k}}^2 + v_{\mathbf{k}}^2)(2u_{\mathbf{p}}v_{\mathbf{p}})] \bar{h}_{\mathbf{k}} + \gamma_{\mathbf{k}-\mathbf{p}} [(u_{\mathbf{k}}^2 + v_{\mathbf{k}}^2)(u_{\mathbf{p}}^2 + v_{\mathbf{p}}^2) - (2u_{\mathbf{k}}v_{\mathbf{k}})(2u_{\mathbf{p}}v_{\mathbf{p}})] h_{\mathbf{k}}, \quad (\text{B8})$$

$$\Delta_{2,\mathbf{k}} = -\frac{2}{N'} \sum_{\mathbf{p}} \gamma_{\mathbf{k}-\mathbf{p}} [(2u_{\mathbf{k}}v_{\mathbf{k}})(2u_{\mathbf{p}}v_{\mathbf{p}}) - (u_{\mathbf{k}}^2 + v_{\mathbf{k}}^2)(u_{\mathbf{p}}^2 + v_{\mathbf{p}}^2)] \bar{h}_{\mathbf{k}} + \gamma_{\mathbf{k}-\mathbf{p}} [(u_{\mathbf{k}}^2 + v_{\mathbf{k}}^2)(2u_{\mathbf{p}}v_{\mathbf{p}}) - (2u_{\mathbf{k}}v_{\mathbf{k}})(u_{\mathbf{p}}^2 + v_{\mathbf{p}}^2)] h_{\mathbf{k}}, \quad (\text{B9})$$

with $\gamma_{\mathbf{k}}$ being the bare quartic vertex (18), $u_{\mathbf{k}}$ and $v_{\mathbf{k}}$ being the Bogoliubov coefficients (24), and $h_{\mathbf{k}}$ and $\bar{h}_{\mathbf{k}}$ being respectively the normal and anomalous expectation values (45).

Again, due to the property (B1), it is useful to define the set of coefficients

$$b_i(i, j) = \frac{1}{N'} \sum_{\mathbf{p}} f_i(\mathbf{p})\bar{g}_j(\mathbf{p}), \quad (\text{B10})$$

where $i, j = 1, 2, 3, 4$ and the functions $\bar{g}_i(\mathbf{p})$ are given in terms of the Bogoliubov coefficients (24) and the normal and anomalous expectation values (45):

$$\begin{aligned}\bar{g}_1(\mathbf{p}) &= (u_{\mathbf{p}}^2 + v_{\mathbf{p}}^2)\bar{h}(\mathbf{p}) = -\frac{A_{\mathbf{p}}\bar{B}_{\mathbf{p}}}{2\omega_{\mathbf{p}}\Omega_{\mathbf{p}}}, & \bar{g}_2(\mathbf{p}) &= 2u_{\mathbf{p}}v_{\mathbf{p}}\bar{h}(\mathbf{p}) = -\frac{B_{\mathbf{p}}\bar{B}_{\mathbf{p}}}{2\omega_{\mathbf{p}}\Omega_{\mathbf{p}}}, \\ \bar{g}_3(\mathbf{p}) &= (u_{\mathbf{p}}^2 + v_{\mathbf{p}}^2)h(\mathbf{p}) = \frac{A_{\mathbf{p}}}{2\omega_{\mathbf{p}}}\left(-1 + \frac{\bar{A}_{\mathbf{p}}}{\Omega_{\mathbf{p}}}\right), & \bar{g}_4(\mathbf{p}) &= 2u_{\mathbf{p}}v_{\mathbf{p}}h(\mathbf{p}) = \frac{B_{\mathbf{p}}}{2\omega_{\mathbf{p}}}\left(-1 + \frac{\bar{A}_{\mathbf{p}}}{\Omega_{\mathbf{p}}}\right).\end{aligned}\quad (\text{B11})$$

Then, it is easy to show that Eqs. (B7)–(B9) can be rewritten as

$$\begin{aligned}E_{44} &= -\frac{3}{4}N \sum_i C_i \left[[b_4(i, 2) - b_4(i, 3)]^2 - [b_4(i, 1) - b_4(i, 4)]^2 \right], \\ \Delta_{1,\mathbf{k}} &= \sum_i C_i \frac{f_i(\mathbf{k})}{\omega_{\mathbf{k}}} [(b_4(i, 3) - b_4(i, 2)) A_{\mathbf{k}} + (b_4(i, 1) - b_4(i, 4)) B_{\mathbf{k}}], \\ \Delta_{2,\mathbf{k}} &= \sum_i C_i \frac{f_i(\mathbf{k})}{\omega_{\mathbf{k}}} [(b_4(i, 4) - b_4(i, 1)) A_{\mathbf{k}} + (b_4(i, 2) - b_4(i, 3)) B_{\mathbf{k}}],\end{aligned}\quad (\text{B12})$$

where C_i are the coefficients (B2), $f_i(\mathbf{k})$ are the functions (B3), $A_{\mathbf{k}}$ and $B_{\mathbf{k}}$ are respectively the coefficients (15) and (16), and $\omega_{\mathbf{k}}$ is the triplon energy (23).

Due to the form of Eq. (B12), we define a new set of coefficients

$$b_1(i) \equiv b_4(i, 4) - b_4(i, 1) = \frac{1}{2N'} \sum_{\mathbf{p}} f_i(\mathbf{p}) \frac{1}{\omega_{\mathbf{p}}\Omega_{\mathbf{p}}} [B_{\mathbf{p}}(\bar{A}_{\mathbf{p}} - \bar{\Omega}_{\mathbf{p}}) + A_{\mathbf{p}}\bar{B}_{\mathbf{p}}], \quad (\text{B13})$$

$$b_2(i) \equiv b_4(i, 3) - b_4(i, 2) = \frac{1}{2N'} \sum_{\mathbf{p}} f_i(\mathbf{p}) \frac{1}{\omega_{\mathbf{p}}\Omega_{\mathbf{p}}} [A_{\mathbf{p}}(\bar{A}_{\mathbf{p}} - \bar{\Omega}_{\mathbf{p}}) + B_{\mathbf{p}}\bar{B}_{\mathbf{p}}], \quad (\text{B14})$$

where $i = 1, 2, 3, 4$, $\bar{A}_{\mathbf{p}}$ and $\bar{B}_{\mathbf{p}}$ are the coefficients (38), and $\bar{\Omega}_{\mathbf{p}}$ is the energy (43) of the elementary excitations above the many-triplon state (47). Finally, we recall Eq. (46) that is related to the condition (39):

$$\frac{\bar{N}}{N} = \frac{3}{4N'} \sum_{\mathbf{k}} \left(-1 + \frac{\bar{A}_{\mathbf{p}}}{\Omega_{\mathbf{p}}} \right). \quad (\text{B15})$$

Equations (B13)–(B15) define a self-consistent problem that is numerically solved for a fixed value of the triplon number \bar{N} and the ratio J_2/J_1 of the exchange couplings. Such set of self-consistent equations allows us to calculate the coefficients $b_1(i)$ and $b_2(i)$, with $i = 1, 2, 3, 4$, and the chemical potential $\bar{\mu}$, yielding the energy (42) and the excitation spectrum (43).

-
- [1] S. Sachdev, in *Quantum Magnetism*, Lecture Notes in Physics Vol. 645, edited by U. Schollwck, J. Richter, D. J. J. Farnell, and R. A. Bishop (Springer, Berlin, 2004); Nat. Phys. **4**, 173 (2008).
 - [2] N. Read and S. Sachdev, Valence-bond and spin-Peierls ground states of low-dimensional quantum antiferromagnets, Phys. Rev. Lett. **62**, 1694 (1989); Spin-Peierls, valence-bond solid, and Néel ground states of low-dimensional quantum antiferromagnets, Phys. Rev. B **42**, 4568 (1990).
 - [3] C. Lacroix, P. Mendels, and F. Mila, editors, *Introduction to Frustrated Magnetism*, Springer Series in Solid-State Sciences 164 (Springer, Berlin, 2011).
 - [4] R. Ganesh, J. van den Brink, and S. Nishimoto, Deconfined Criticality in the Frustrated Heisenberg Honeycomb Antiferromagnet, Phys. Rev. Lett. **110**, 127203 (2013).
 - [5] Z. Zhu, D. A. Huse, and S. R. White, Weak Plaquette Valence Bond Order in the S=1/2 Honeycomb J_1 – J_2 Heisenberg Model, Phys. Rev. Lett. **110**, 127205 (2013).
 - [6] For more details about the J_1 – J_2 model on the honeycomb lattice see, e.g., the Introduction section of F. Ferrari, S. Bieri, and F. Becca, Competition between spin liquids and valence-bond order in the frustrated spin-1/2 Heisenberg model on the honeycomb lattice, Phys. Rev. B **96**, 104401 (2017).
 - [7] J. Marston and C. Zeng, SpinPeierls and spinliquid phases of Kagom quantum antiferromagnets, J. Appl. Phys. **69**, 5962 (1991).
 - [8] B.-J. Yang, Y. B. Kim, J. Yu, and K. Park, Spin triplet excitations for a valence bond solid on the kagome lattice,

- Phys. Rev. B **77**, 224424 (2008).
- [9] For additional references about VBS states on the kagome lattice see, e.g., the Introduction section of K. Hwang, Y. Huh, and Y. B. Kim, Z_2 gauge theory for valence bond solids on the kagome lattice, Phys. Rev. B **92**, 205131 (2015).
 - [10] Y.-C. He, M. P. Zaletel, M. Oshikawa, and F. Pollmann, Signatures of Dirac Cones in a DMRG Study of the Kagome Heisenberg Model, Phys. Rev. X **7**, 031020 (2017).
 - [11] L. Savary and L. Balents, Quantum spin liquids: a review, Rep. Prog. Phys. **80**, 016502 (2017).
 - [12] Y. Zhou, K. Kanoda, and T.-K. Ng, Quantum spin liquid states, Rev. Mod. Phys. **89**, 025003 (2017).
 - [13] A. W. Sandvik, Evidence for Deconfined Quantum Criticality in a Two-Dimensional Heisenberg Model with Four-Spin Interactions, Phys. Rev. Lett. **98**, 227202 (2007).
 - [14] A. W. Sandvik, Continuous Quantum Phase Transition between an Antiferromagnet and a Valence-Bond Solid in Two Dimensions: Evidence for Logarithmic Corrections to Scaling, Phys. Rev. Lett. **104**, 177201 (2010).
 - [15] A. W. Sandvik, Finite-size scaling and boundary effects in two-dimensional valence-bond solids, Phys. Rev. B **85**, 134407 (2012).
 - [16] H. Suwa, A. Sen, and A. W. Sandvik, Level spectroscopy in a two-dimensional quantum magnet: Linearly dispersing spinons at the deconfined quantum critical point, Phys. Rev. B **94**, 144416 (2016).
 - [17] See, e.g., P. Henelius and A. W. Sandvik, Sign problem in Monte Carlo simulations of frustrated quantum spin systems, Phys. Rev. B **62**, 1102 (2000).
 - [18] T. Senthil, L. Balents, S. Sachdev, A. Vishwanath, and M. P. A. Fisher, Quantum criticality beyond the Landau-Ginzburg-Wilson paradigm, Phys. Rev. B **70**, 144407 (2004).
 - [19] S. Sachdev and R. Bhatt, Bond-operator representation of quantum spins: Mean-field theory of frustrated quantum Heisenberg antiferromagnets, Phys. Rev. B **41**, 9323 (1990).
 - [20] A. Auerbach, *Interacting Electrons and Quantum Magnetism* (Springer-Verlag, New York, 1994).
 - [21] R. L. Doretto and M. Vojta, Triangular-lattice anisotropic dimerized Heisenberg antiferromagnet: Stability and excitations of the quantum paramagnetic phase, Phys. Rev. B **85**, 104416 (2012).
 - [22] R. L. Doretto, Plaquette valence-bond solid in the square-lattice J_1 - J_2 antiferromagnet Heisenberg model: A bond operator approach, Phys. Rev. B **89**, 104415 (2014).
 - [23] L. S. G. Leite and R. L. Doretto, Entanglement entropy for the valence bond solid phases of two-dimensional dimerized Heisenberg antiferromagnets, Phys. Rev. B **100**, 045113 (2019).
 - [24] L. Wang, Z.-C. Gu, F. Verstraete, and X.-G. Wen, Tensor-product state approach to spin-1/2 square J_1 - J_2 antiferromagnetic Heisenberg model: Evidence for deconfined quantum criticality, Phys. Rev. B **94**, 075143 (2016).
 - [25] A. Yu. Aktersky and A. V. Syromyatnikov, Low-energy singlet sector in the spin-1/2 J_1 - J_2 Heisenberg model on a square lattice, J. Exp. Theor. Phys. **123** 1035 (2016).
 - [26] A. V. Syromyatnikov and A. Yu. Aktersky, Elementary excitations in the ordered phase of spin-1/2 J_1 - J_2 model on square lattice, Phys. Rev. B **99**, 224402 (2019).
 - [27] K. Choo, T. Neupert, and G. Carleo, Two-dimensional frustrated J_1 - J_2 model studied with neural network quantum states, Phys. Rev. B **100**, 125124 (2019).
 - [28] D. Roscher, N. Gneist, M. M. Scherer, S. Trebst, and S. Diehl, Cluster functional renormalization group and absence of a bilinear spin liquid in the J_1 - J_2 Heisenberg model, Phys. Rev. B **100**, 125130 (2019).
 - [29] V. N. Kotov, J. Oitmaa, O. P. Sushkov, and W. H. Zheng, Low-energy singlet and triplet excitations in the spin-liquid phase of the two-dimensional J_1 - J_2 model, Phys. Rev. B **60**, 14613 (1999).
 - [30] R. Haghshenas and D. N. Sheng, U(1)-symmetric infinite projected entangled-pair states study of the spin-1/2 square J_1 - J_2 Heisenberg model, Phys. Rev. B **97**, 174408 (2018).
 - [31] A. Metavitsiadis, D. Sellmann, and S. Eggert, Spin-liquid versus dimer phases in an anisotropic J_1 - J_2 frustrated square antiferromagnet, Phys. Rev. B **89**, 241104(R) (2014).
 - [32] M. E. Zhitomirsky and K. Ueda Valence-bond crystal phase of a frustrated spin-1/2 square-lattice antiferromagnet, Phys. Rev. B **54**, 9007 (1996).
 - [33] S.-S. Gong, W. Zhu, D. N. Sheng, O. I. Motrunich, and M. P. A. Fisher, Plaquette Ordered Phase and Quantum Phase Diagram in the Spin-1/2 J_1 - J_2 Square Heisenberg Model, Phys. Rev. Lett. **113**, 027201 (2014).
 - [34] A. Ralko, M. Mambrini, and D. Poilblanc, Generalized quantum dimer model applied to the frustrated Heisenberg model on the square lattice: Emergence of a mixed columnar-plaquette phase, Phys. Rev. B **80**, 184427 (2009).
 - [35] J. Richter, R. Zinke, and D. J. J. Farnell, The spin-1/2 square-lattice J_1 - J_2 model: the spin-gap issue, Eur. Phys. J. B **88** 2 (2015).
 - [36] L. Wang and A. W. Sandvik, Critical Level Crossings and Gapless Spin Liquid in the Square-Lattice Spin-1/2 J_1 - J_2 Heisenberg Antiferromagnet, Phys. Rev. Lett. **121**, 107202 (2018).
 - [37] F. Ferrari and F. Becca, Spectral signatures of fractionalization in the frustrated Heisenberg model on the square lattice, Phys. Rev. B **98**, 100405(R) (2018).
 - [38] W.-Y. Liu, S. Dong, C. Wang, Y. Han, H. An, G.-C. Guo, and L. He, Gapless spin liquid ground state of the spin-1/2 J_1 - J_2 Heisenberg model on square lattices, Phys. Rev. B **98**, 241109(R) (2018).
 - [39] X. Yang and F. Wang, Schwinger boson spin-liquid states on square lattice, Phys. Rev. B **94**, 035160 (2016).
 - [40] For more details about the J_1 - J_2 model on the square lattice, we refer the reader, e.g., to the Introduction section of Ref. [22] and the references therein.
 - [41] T. Grover, Y. Zhang, and A. Vishwanath, Entanglement entropy as a portal to the physics of quantum spin liquids, New J. Phys. **15** 025002 (2013).
 - [42] N. Laflorencie, Quantum entanglement in condensed matter systems, Phys. Rep. **646**, 1 (2016).
 - [43] J. Eisert, M. Cramer, and M. B. Plenio, Colloquium: Area laws for the entanglement entropy Rev. Mod. Phys. **82**, 277 (2010).
 - [44] A. F. Albuquerque and F. Alet, Critical correlations for short-range valence-bond wave functions on the square lattice, Phys. Rev. B **82**, 180408(R) (2010).
 - [45] Y. Tang, A. W. Sandvik, and C. L. Henley, Properties of resonating-valence-bond spin liquids and critical dimer

- models, Phys. Rev. B **84**, 174427 (2011).
- [46] J. Wildeboer and A. Seidel, Correlation Functions in SU(2)-Invariant Resonating-Valence-Bond Spin Liquids on Nonbipartite Lattices, Phys. Rev. Lett. **109**, 147208 (2012).
 - [47] F. Yang and H. Yao, Frustrated Resonating Valence Bond States in Two Dimensions: Classification and Short-Range Correlations, Phys. Rev. Lett. **109**, 147209 (2012).
 - [48] J. Wildeboer, A. Seidel, and R. G. Melko, Entanglement entropy and topological order in resonating valence-bond quantum spin liquids, Phys. Rev. B **95**, 100402(R) (2017).
 - [49] S. Hu, W. Zhu, S. Eggert, and Y.-C. He, Dirac Spin Liquid on the Spin-1/2 Triangular Heisenberg Antiferromagnet, Phys. Rev. Lett. **123**, 207203 (2019).
 - [50] Z. Zhu and S. R. White, Spin liquid phase of the spin $S=1/2$ J_1 - J_2 Heisenberg model on the triangular lattice, Phys. Rev. B **92**, 041105(R) (2015).
 - [51] W.-J. Hu, S.-S. Gong, W. Zhu, and D. N. Sheng, Competing spin-liquid states in the spin-1/2 Heisenberg model on the triangular lattice, Phys. Rev. B **92**, 140403(R) (2015).
 - [52] S. N. Saadatmand and I. P. McCulloch, Symmetry fractionalization in the topological phase of the spin-1/2 J_1 - J_2 triangular Heisenberg model, Phys. Rev. B **94**, 121111(R) (2016).